The Application of Crustal Models in Regional Modelling of the Earth's Gravity Field

Matej Varga

Faculty of Geodesy, University of Zagreb
Supervisors: Prof. Tomislav Bašić, PhD
Prof. Dimitrios Tsoulis, PhD

Introduction

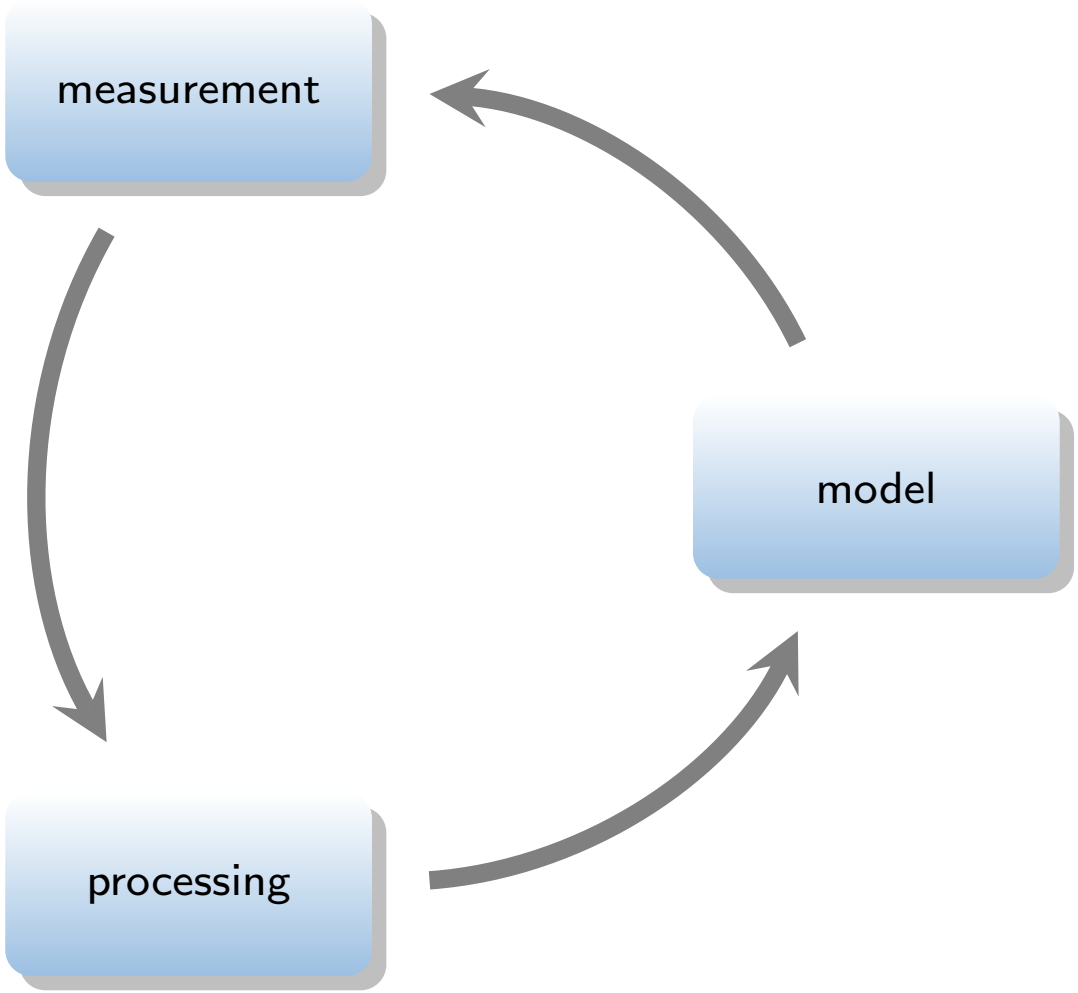

Motivation

#1

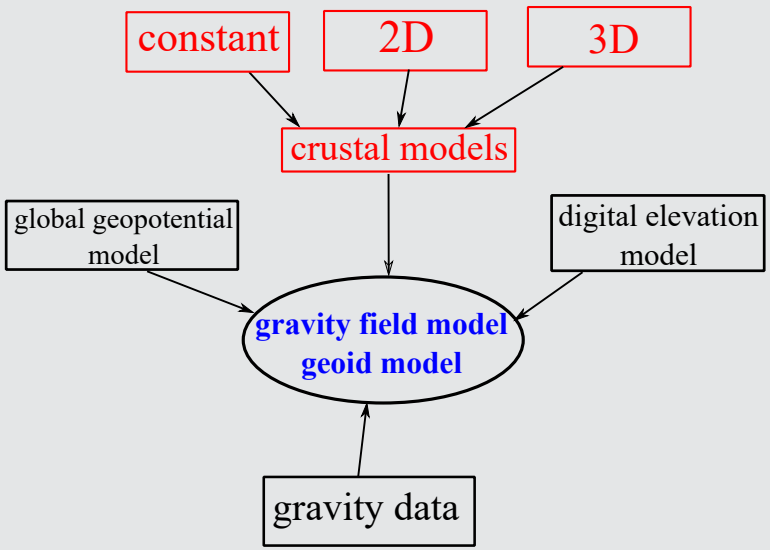

2

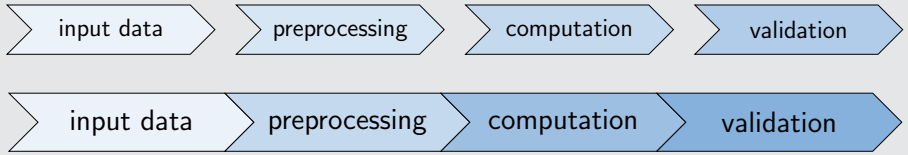

3

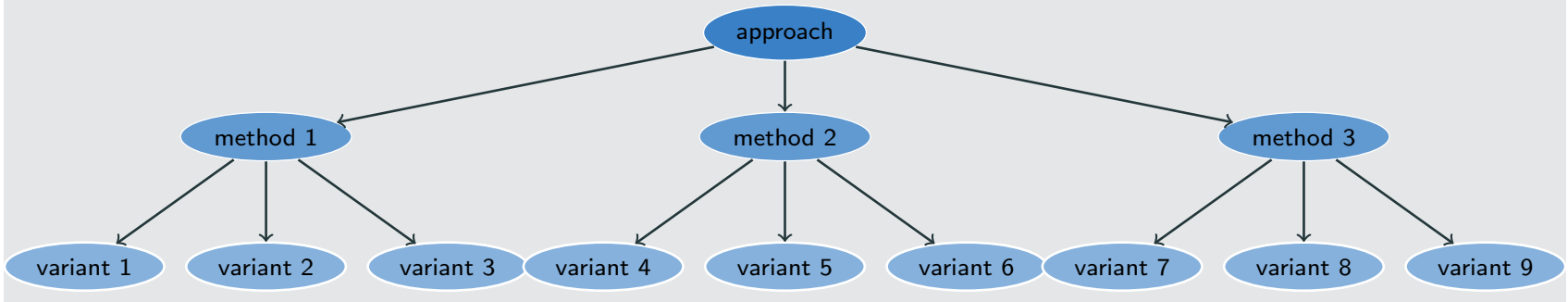

Topographic reductions

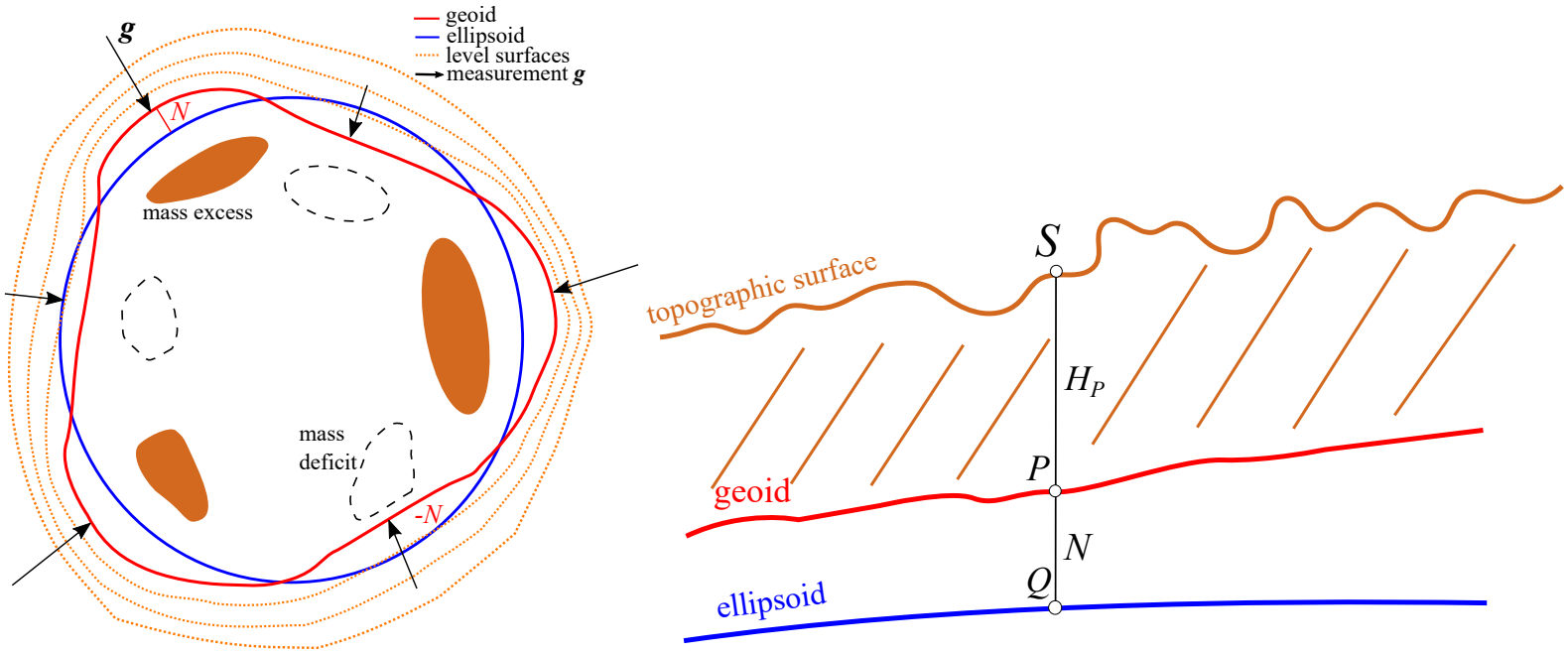

(a) The principle of gravity field modeling and geoid determination

(b) Topographic reduction

Figure 1

Gravity anomaly	Symbol	Indirect effects on N	Smoothness	Geophysical interpretation
Free-Air	Δg_{FA}	large	very rough	yes
Bouguer	Δg_{B}	very large	smooth	yes
Faye	Δg_{Faye}	very small	rough	no
Airy-Heiskanen	Δg_{A-H}	small	smooth	yes
Pratt-Hayford	Δg_{P-H}	small	smooth	yes
RTM	Δg_{RTM}	very small	smooth	no

Table 1: Properties of the gravity anomaly types for different reduction schemes

Topographic reductions

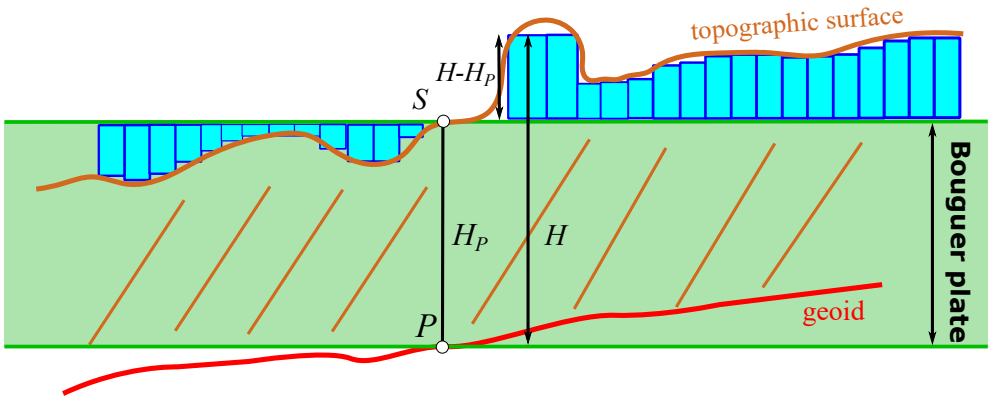

Figure 2: Terrain correction

Terrain correction

$$\delta g_{TC} = G \int \int \int_{H}^{H_P} \frac{\rho(x,y,z)(H_P - H)}{l^3} dxdydz$$

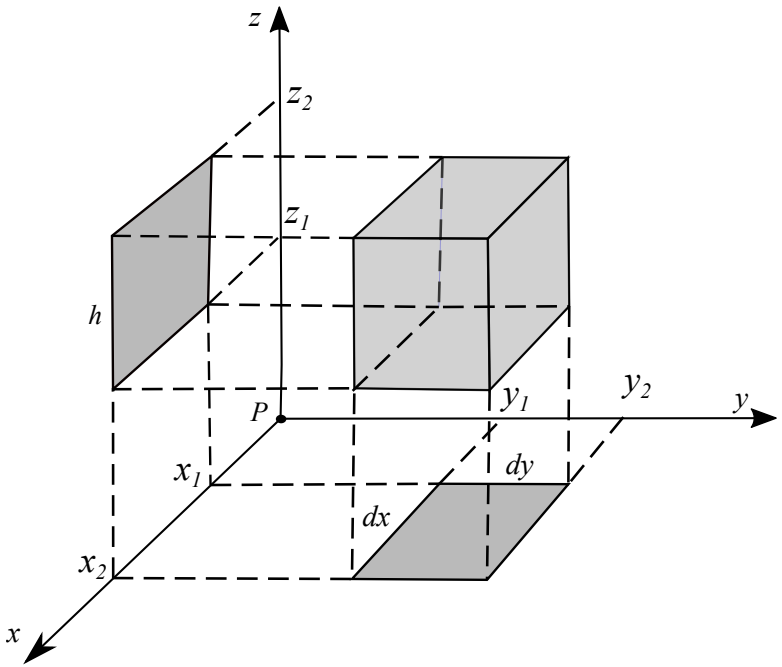

Figure 3: Rectangular prism (Nagy, 1966)

Rectangular prism solution for terrain correction

$$\delta g_{TC} = G\rho \left| \left| \left| x \ln(y + r) + y \ln(x + r) - z \arctan \frac{xy}{zr} \right|_{x_1}^{x_2} \right|_{y_1}^{y_2} \right|_{z_1}^{z_2}$$

Topographic reductions and density

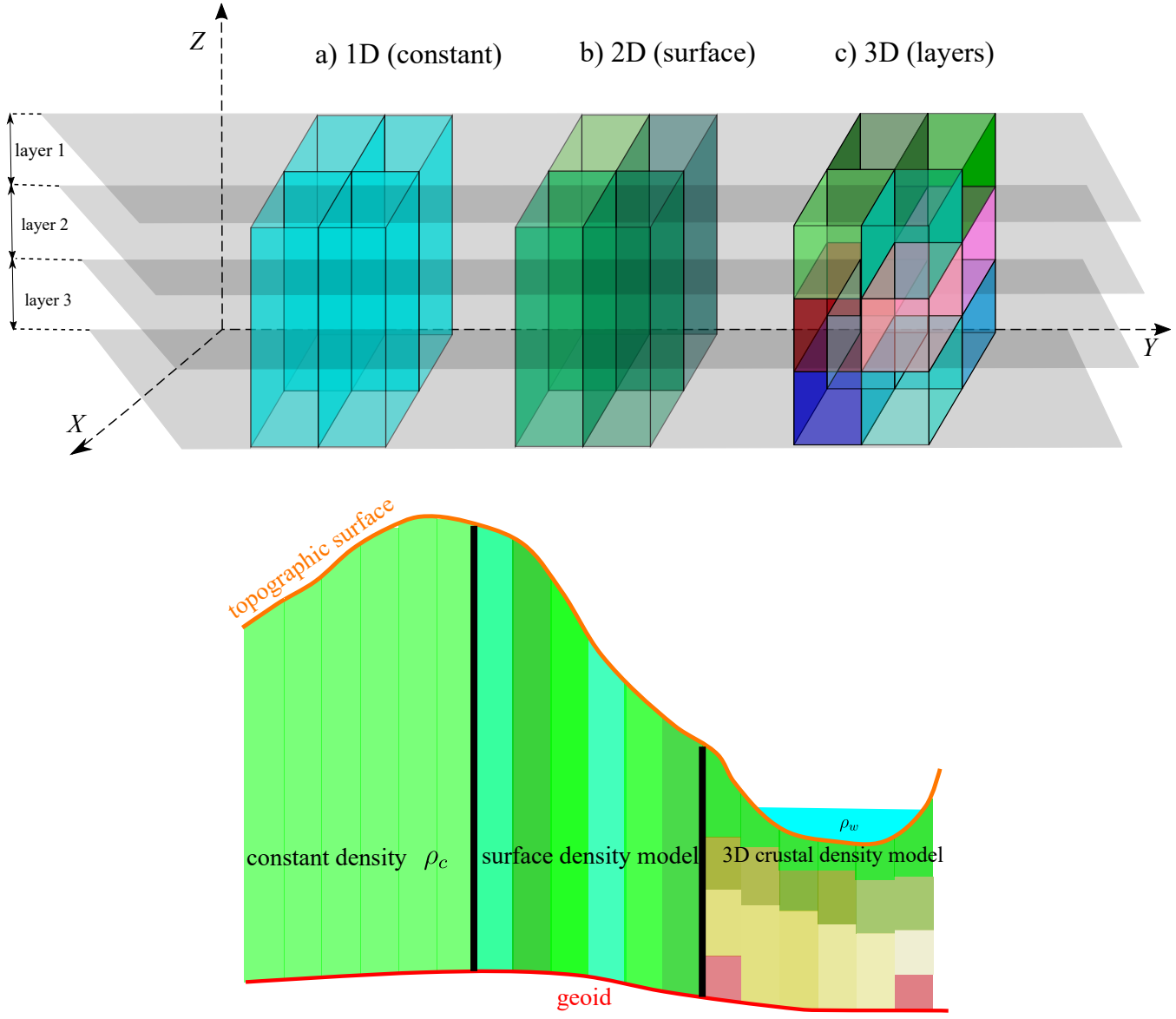

Figure 4: Rectangular prisms for three cases: a) ρ_C, b) surface crustal density model, and c) 3D crustal density model (Brkić, 1994)

Why the geoid?

Classical levelling

$\Delta H = \mathrm{B} - \mathrm{F}$

$H_2 = H_1 + \Delta H$

GNSS/levelling

$H_1 = h_1 - N_1,$

$H_2 = h_2 - N_2$

$\Delta H = H_2 - H_1$

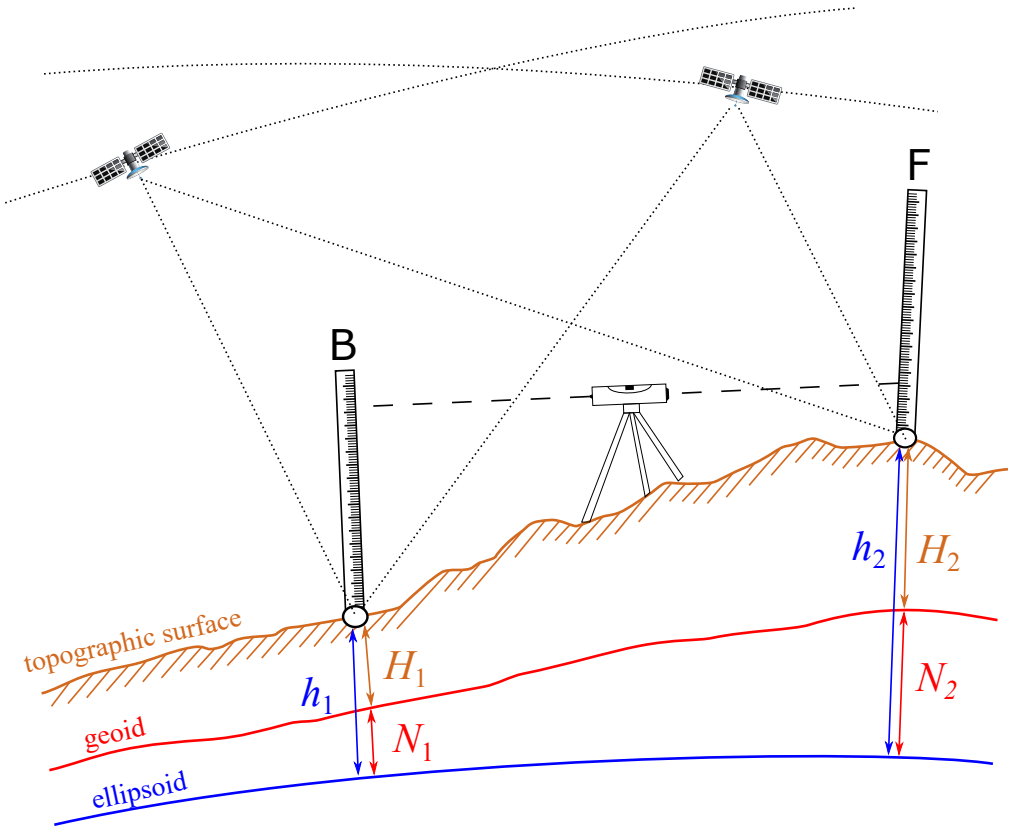

Figure 5: Classical levelling and GNSS/levelling (Gerlach, 2003)

Geoid determination approaches

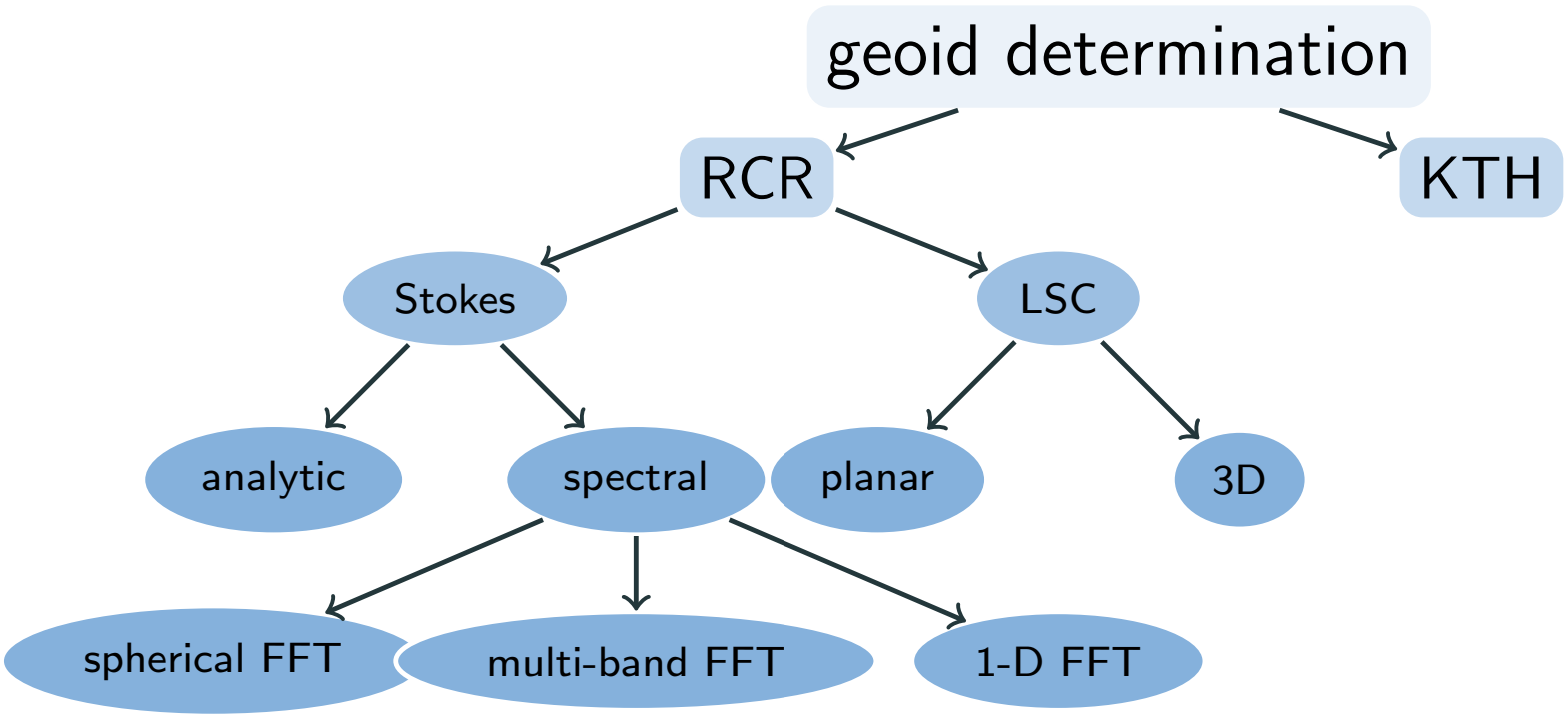

Geoid determination approaches: remove-compute-restore

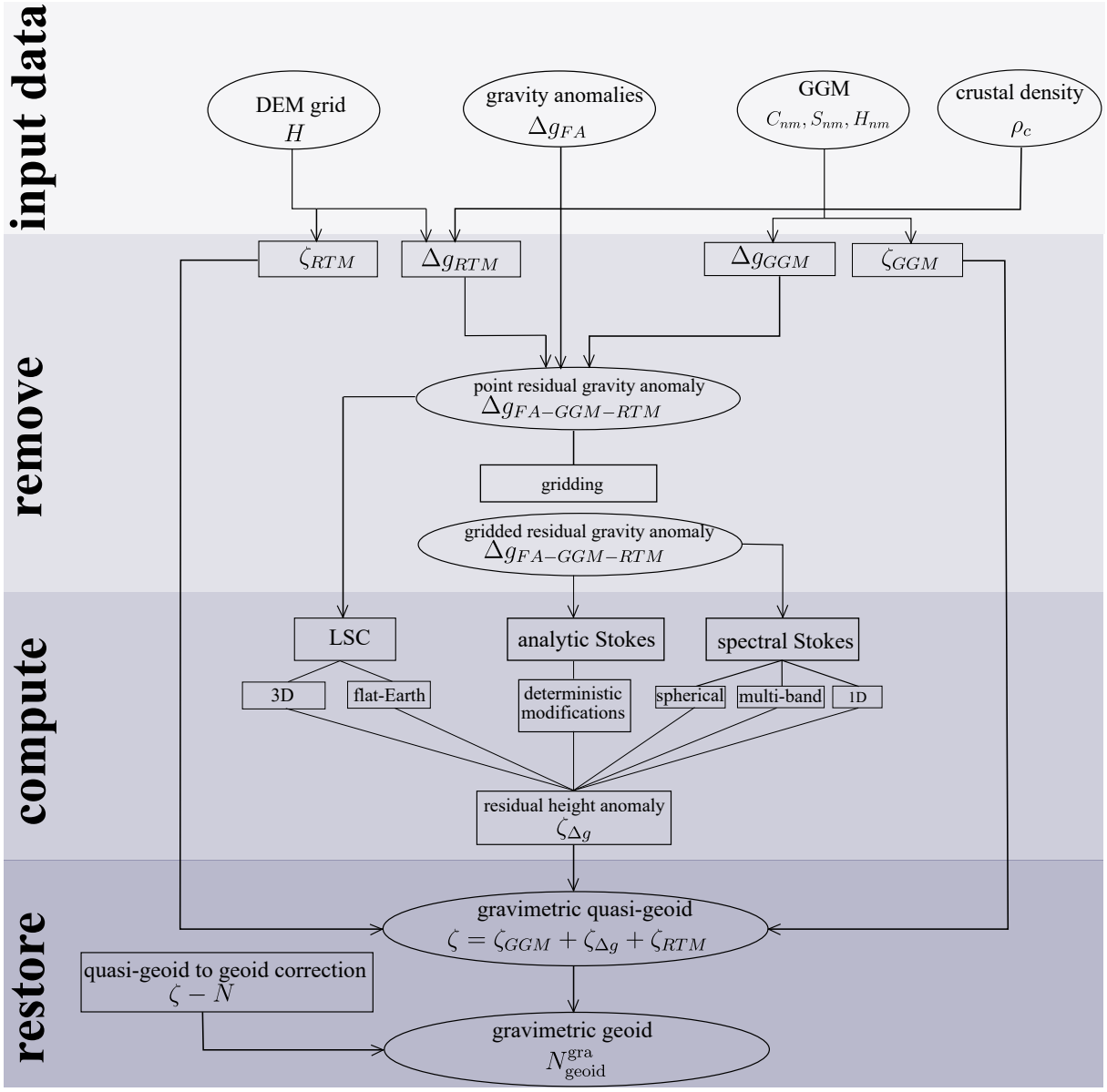

Figure 6: Flowchart of geoid determination with RCR approach

Geoid determination approaches: RCR, Stokes

Stokes integral

$$N = \frac{R}{4\pi\gamma} \iint S(\psi)\Delta g d\sigma$$

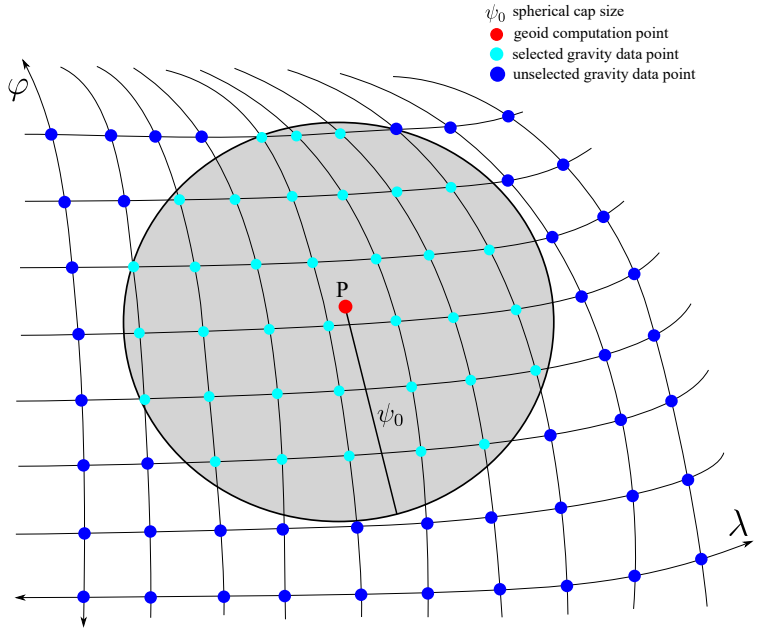

Figure 7: Stokes' integration

Forms of Stokes kernel

$$\text{spectral} : S(\psi) = \sum_{n=2}^{\infty} \frac{2n+1}{n-1} P_n \cos\psi$$

$$\text{closed} : S(\psi) = \frac{1}{s} - 6s + 1 - 5\cos\psi - 3\cos\psi \ln(s + s^2),\ s = \sin\frac{1}{2}\psi$$

$$\text{planar} : S(\psi) \approx \frac{1}{\sin\frac{\psi}{2}} \approx \frac{2}{\psi} \approx \frac{2R}{l}$$

$$\text{det.modif} : S^L(\psi) = \sum_{n=2}^{\infty} \frac{2n+1}{n-1} P_n(\cos\psi) - \sum_{n=2}^{L} \frac{2n+1}{2} s_n P_n(\cos\psi)$$

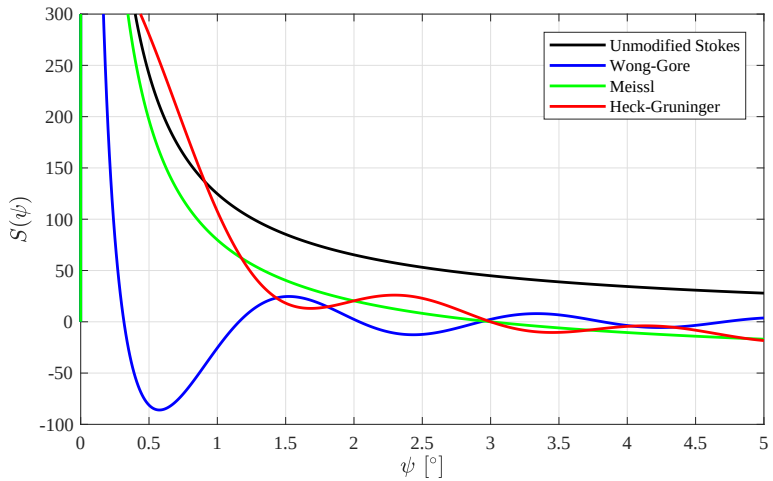

Figure 8: Stokes' kernel $S(\psi)$ modifications as a function of the spherical distance ψ.

Geoid determination approaches: KTH

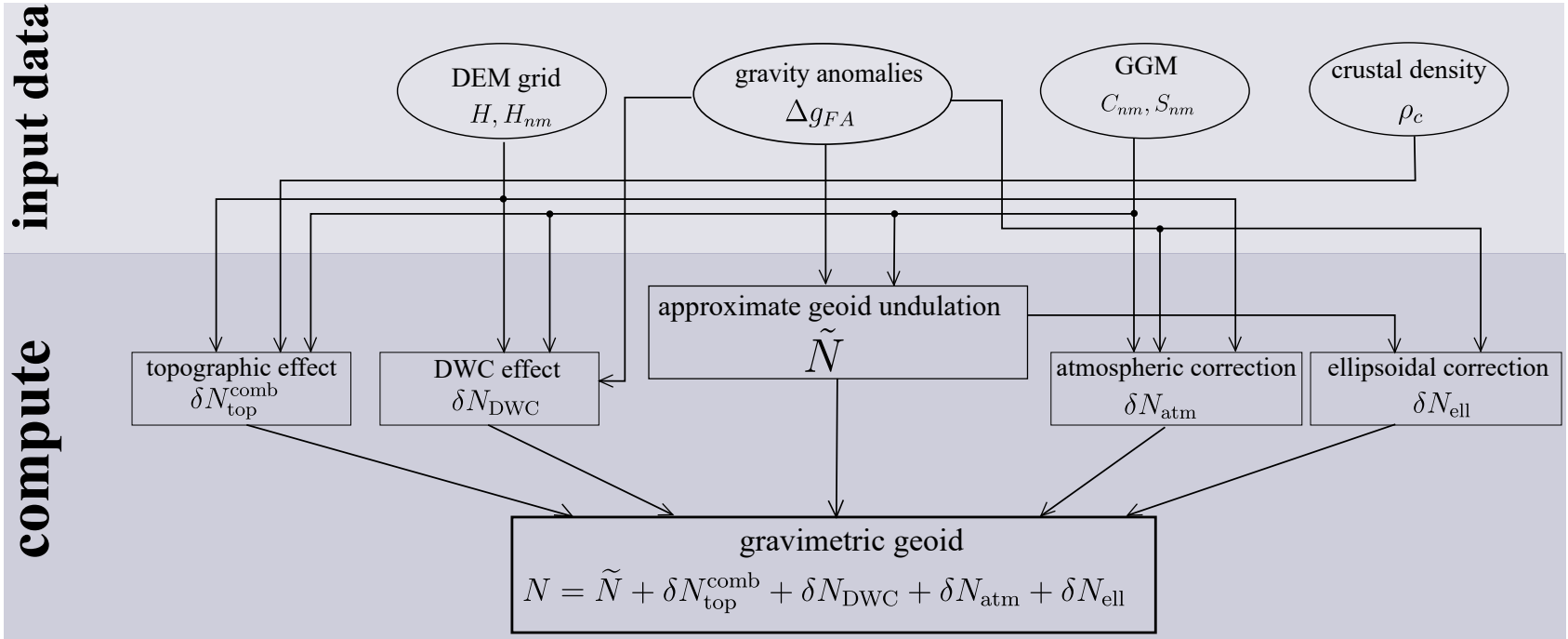

Figure 9: Flowchart of geoid determination with KTH approach.

Formulas

$$\tilde{N} = \frac{R}{4\gamma} \iint_{\sigma_0} S^L(\psi) \Delta g \, d\sigma + \frac{R}{2\gamma} \sum_{n=2}^{M} b_n \Delta g_n^{GGM}$$

$$\delta N_{\text{top}}^{\text{comb}} = \delta N_{\text{dir}} + \delta N_{\text{ind}}^{\text{top}} = -\frac{2\pi G \rho}{\gamma} \left(H^2 + \frac{2H^3}{3R} \right)$$

$$\delta N_{\text{DWC}} = \delta N_{\text{DWC}}^{(1)} + \delta N_{\text{DWC}}^{L1,Far} + \delta N_{\text{DWC}}^{L2}$$

$$\delta N_{\text{atm}} = -\frac{2\pi R \rho_0}{\gamma} \sum_{n=2} M \left(\frac{2}{n-1} - s_n - Q_n^L \right) H_n - \frac{2\pi R \rho_0}{\gamma} \sum_{n=M+1}^{\infty} \left(\frac{2}{n-1} - \frac{n+2}{2n+1} Q_n^L \right) H_n$$

$$\delta N_{\text{ell}} \approx \psi_0 \left[(0.12 - 0.38 \cos^2 \theta) \Delta g + 0.17 \tilde{N} \sin^2 \theta \right]$$

Geoid model accuracy validation

The main equation

$$\delta N^i_{\text{GNSS/lev.-geoid}} = (h^i_{GNSS} - H^i_{lev.}) - N^i_{\text{geoid}} = N^i_{\text{GNSS/lev.}} - N^i_{\text{geoid}}$$

Condition

$$\delta N^i_{\text{GNSS/lev.-geoid}} \approx 0$$

General equation of parametric models

$$\delta N^i_{\text{GNSS/lev.-geoid}} = N^i_{\text{GNSS/lev.}} - N^i_{\text{geoid}} = A_i^T x + v_i$$

Sources of errors

- Computed geoid undulation
- Computed geoidal height difference
- Orthometric height
- Orthometric height differences
- GPS height and height differences

Name	$\mathbf{A_i^T}$
1-p	1
3-p (1^{st} poly)	1, $\Delta\varphi$, $\Delta\lambda$
5-p	1, $\cos\varphi\cos\lambda$, $\cos\varphi\sin\lambda$, $\sin\varphi$, $\sin^2\varphi$
2^{nd} poly.	1, $\Delta\varphi$, $\Delta\lambda$, $\Delta\varphi\Delta\lambda$, $\Delta\varphi^2$, $\Delta\lambda^2$
3^{rd} poly.	1, $\Delta\varphi$, $\Delta\lambda$, $\Delta\varphi\Delta\lambda$, $\Delta\varphi^2$, $\Delta\lambda^2$, $\Delta\varphi\Delta\lambda^2$, $\Delta\varphi^3$, $\Delta\lambda^3$

Table 2: A list of parametric models (Fotopoulos, 2013)

Description	st. dev.
Highest accuracy	< 1 cm
High	$1 - 3$ cm
Moderate	$4 - 10$ cm
Low	$10 - 20$ cm
Lowest	> 20 cm

Table 3: Geoid model accuracy categories

Previous geoid models in Croatia

Stats and info	HRG2000	HRG2009 (Bašić & Bjelotomić, 2014)	HRG2015 (Bjelotomić, 2015)
min [cm]	-27.5	-7.8	-11.8
max [cm]	24.2	5.8	15.8
mean [cm]	-2.4	-1.2	0.4
st. dev. [cm]	11.4	3.5	4.7
comp. method	RCR/LSC	RCR/LSC	KTH
no. gravity points	7500	$\sim$ 29300	$\sim$ 28000
no. GNSS/lev.	59	59	59

Study area

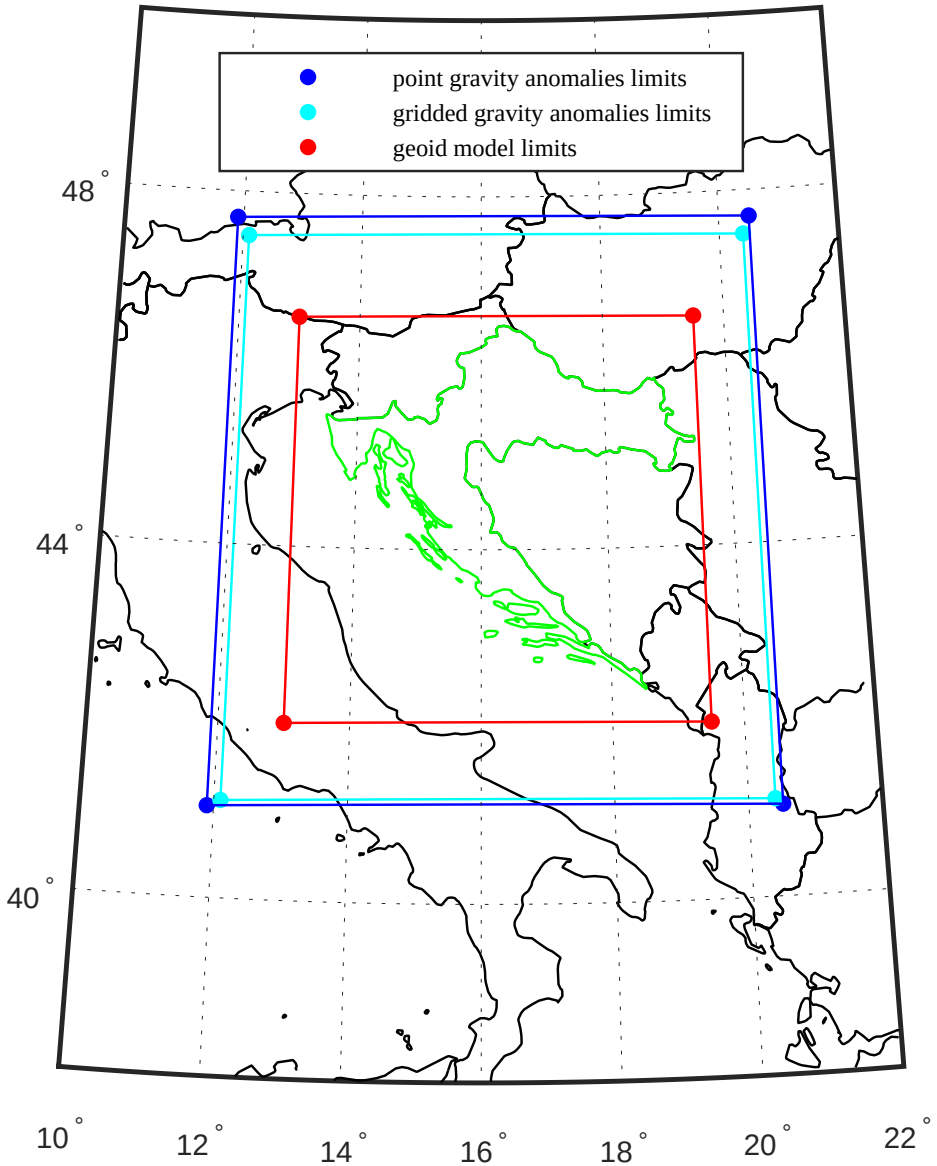

Figure 10: Study area

Gravity anomalies: filtering

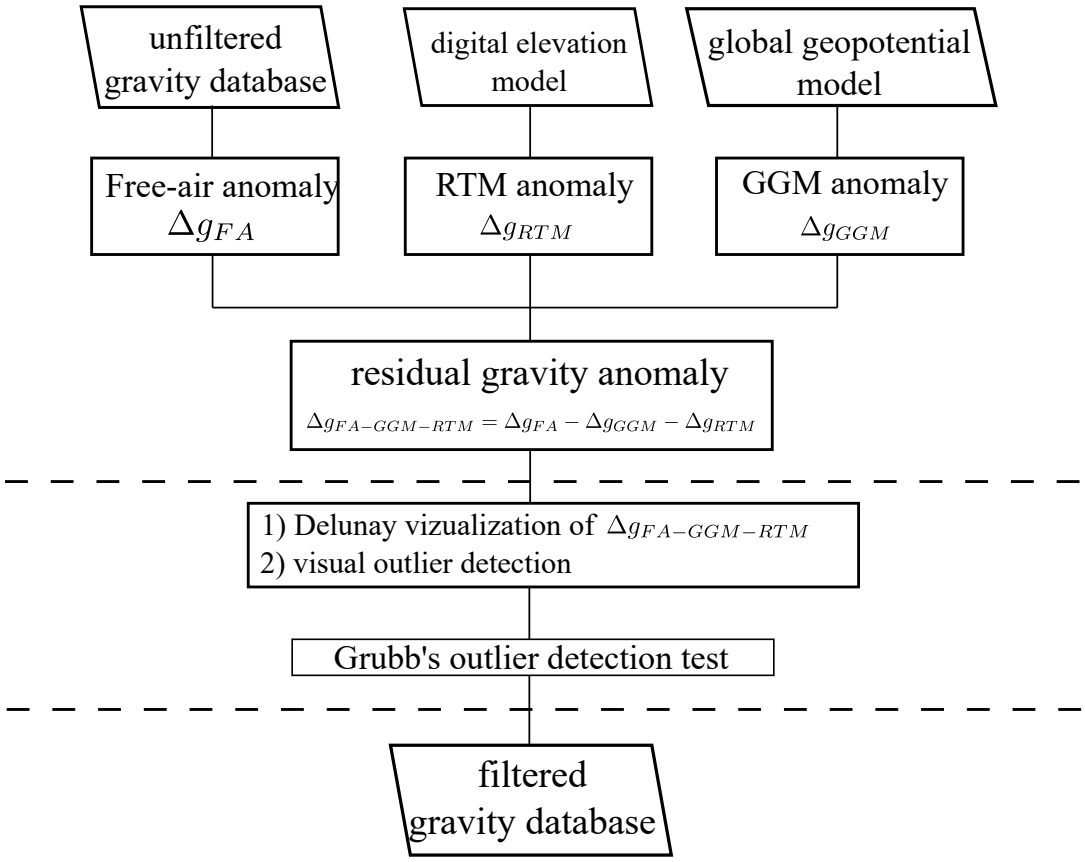

(a) Schematic diagram

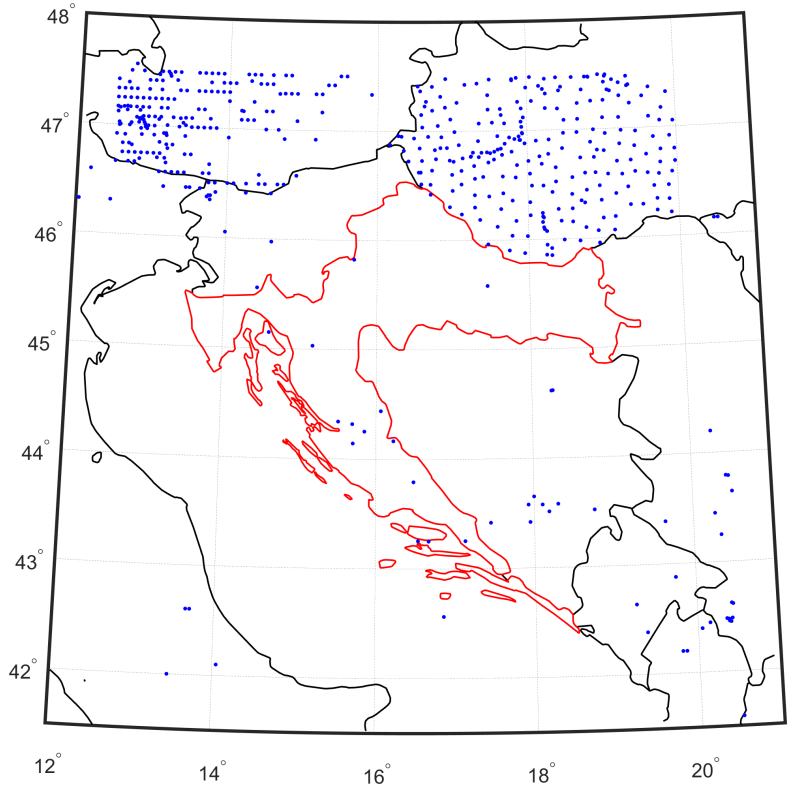

(b) Filtered points

Figure 11

Gravity anomalies: filtering

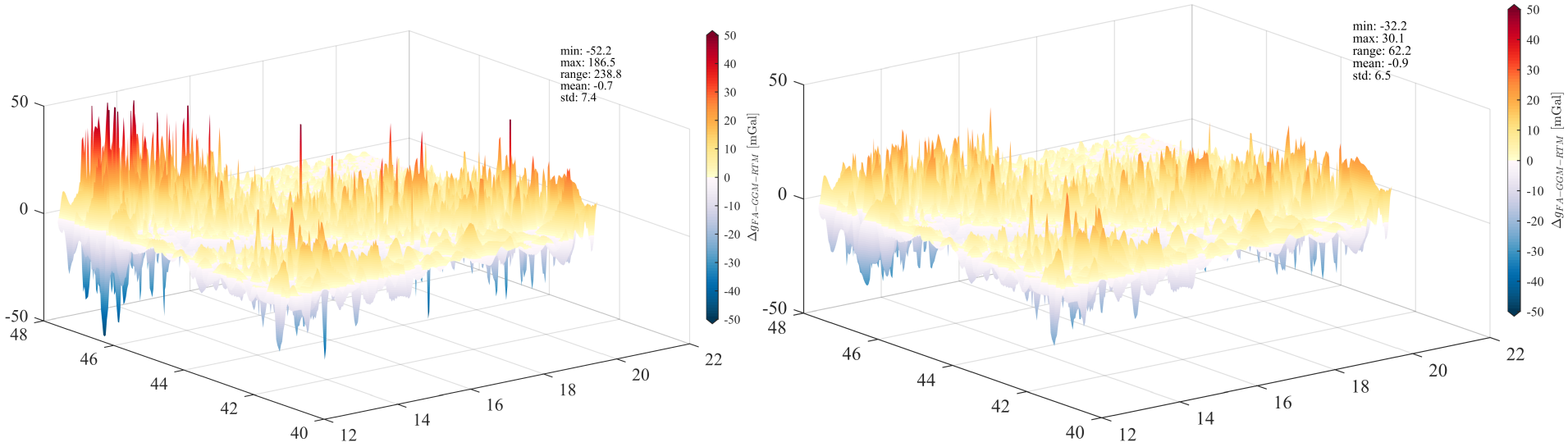

(a) before (b) after

Figure 12: Map of residual gravity anomalies $\Delta g_{FA-GGM-RTM}$

	Δg_{FA}		Δg_{sB}		Δg_{cB}		$\Delta g_{FA-GGM-RTM}$	
	before	after	before	after	before	after	before	after
min	-131	-131	-232	-207	-203	-177	-52.2	-32.2
max	217	217	109	109	111	111	186.5	30.1
range	347	347	341	316	314	288	238.8	62.2
mean	10	10	-28	-28	-25	-25	-0.7	-0.9
st. dev.	35	35	39	38	36	35	7.4	6.5

Table 4: Statistics before and after filtering. Units: [mgal].

Gravity anomalies: gridding

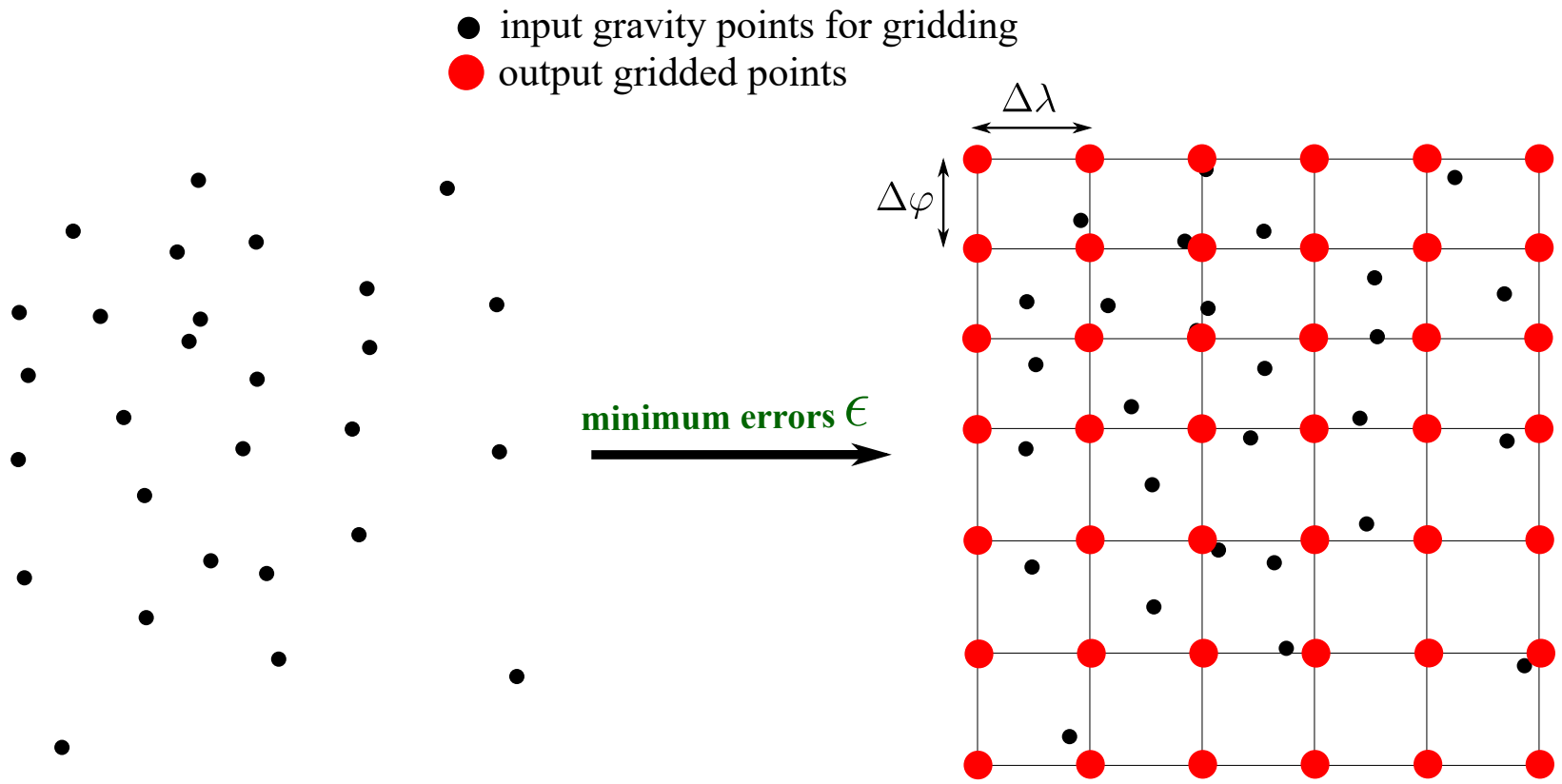

Considerations

- Which type of gravity anomalies to grid?
- Which gridding method to use?
- Error of interpolation ε = known value − gridded value?

Gravity anomalies: gridding

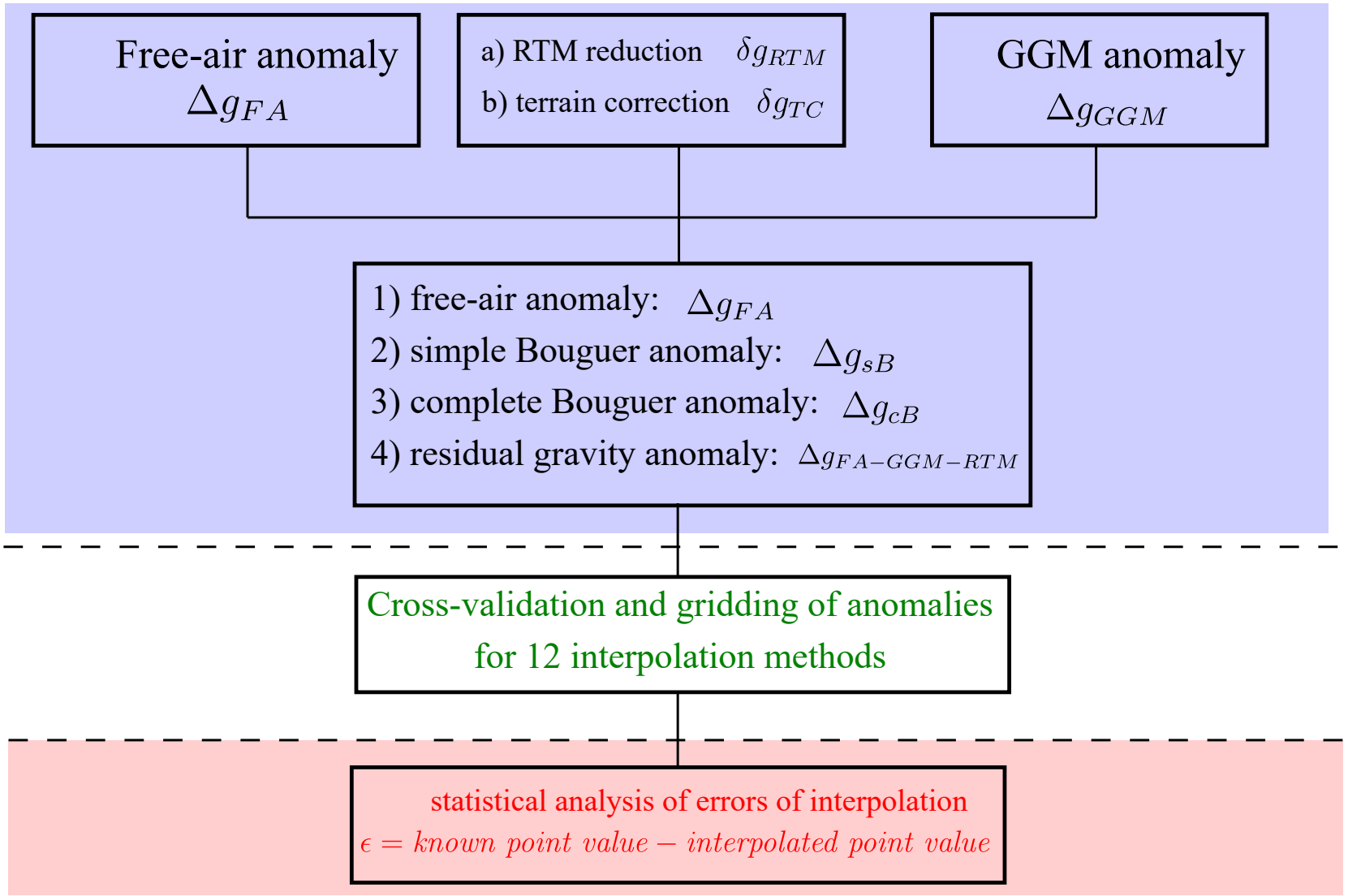

Figure 13: Schematic diagram of the gridding procedure

Gravity anomalies: gridding

Gridding method	min	max	mean	st.dev.
Kriging	-6.3	8.4	0.0	2.1
Inverse Distance to a Power	-13.7	6.5	-0.2	2.8
Radial Basis Function	-10.0	8.0	0.5	2.8
TIN	-11.2	6.4	-0.1	2.9
Minimum Curvature	-6.7	9.8	0.3	3.1
Natural Neighbour	-13.7	11.6	0.2	3.1
Nearest Neighbour	-11.3	10.7	0.5	3.4
Local Polynomial	-10.9	10.2	0.3	3.5
Modified Shepard's	-22.0	31.0	0.2	7.1
Polynomial Regression	-57.0	46.5	-3.4	19.0
Moving Average	-48.2	84.8	1.6	32.4

Table 5: Gridding accuracy of complete Bouguer anomalies Δg_{cB}. Units: [mGal].

Gravity anomaly	Symbol	Interpol.method.	min	max	mean	st.dev.
complete Bouguer	Δg_{cB}	Kriging	-6.3	8.4	0.0	2.1
simple Bouguer	Δg_{sB}	Kriging	-5.8	8.8	0.0	2.3
residual	$\Delta g_{FA} - \Delta g_{GGM} - \Delta g_{RTM}$	Kriging	-5.9	9.4	0.1	3.3
free-air	Δg_{FA}	Kriging	-34.3	21.8	1.6	7.7

Table 6: Comparison of the best interpolation methods for different types of gravity anomalies. Sorted by st.dev. Units: [mGal].

Global geopotential models (GGM)

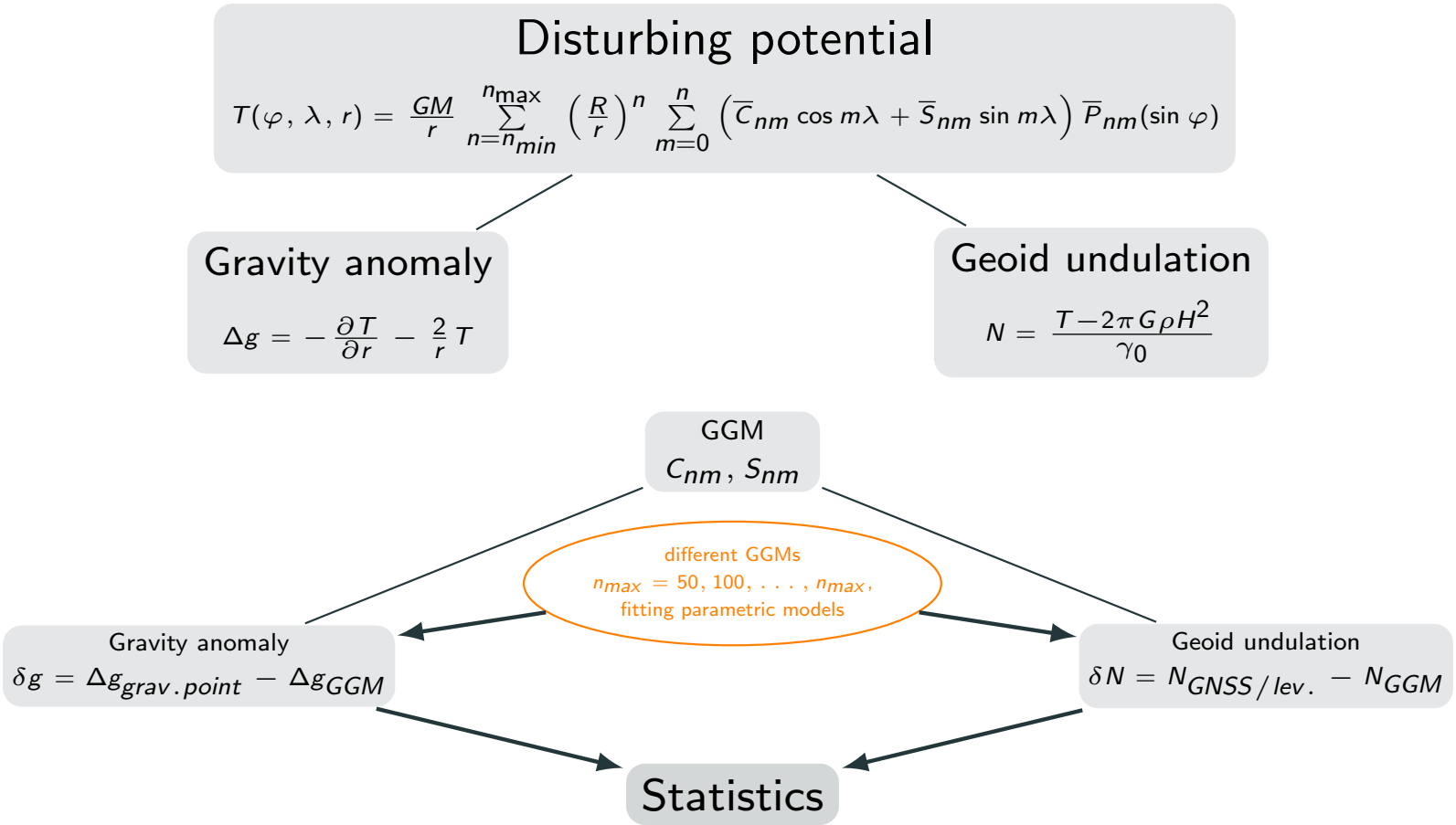

Considerations

- How well do global geopotential models represent *true* gravity field?
- Which GGM model to select in gravity field modelling?
- When to truncate (n_{max})?

Global geopotential models validation

GGM	n_{max}	min	max	mean	st. dev.
eigen-6c4	2190	-150.9	76.1	-5.8	18.2
geco	2190	-138.7	73.1	-6.2	18.2
egm2008	2050	-151.9	72.8	-5.9	18.7
XGM2016	650	-187.8	134.7	-7.3	24.4
goco05c	700	-186.7	139.0	-7.0	24.7
egm96	340	-149.9	136.0	-8.5	26.5
gif48	350	-165.5	104.0	-7.5	27.0
ggm05c	360	-167.8	154.2	-7.9	27.3
ITU-GGC16	230	-168.0	112.8	-7.3	28.4
go-cons-gcf-2-tim-r5	260	-179.1	169.8	-7.9	28.4
NULP-02s	230	-169.8	110.2	-7.9	28.6
goco05s	280	-183.5	112.9	-7.1	28.8
eigen-6s4-v2	210	-166.2	167.6	-7.4	28.9
HUST-Grace2016s	160	-143.5	127.8	-6.0	29.3
ITSG-Grace2014s	170	-146.8	119.6	-7.0	29.2
ITU-GRACE16	150	-141.7	121.8	-5.9	30.0
Tongji-Grace02s	160	-143.3	115.5	-5.8	30.0

Table 7: Statistics of $\delta g = \Delta g_{gravim.point} - \Delta g_{GGM}$. Units: [mGal].

GGM	n_{max}	min	max	mean	st. dev.
egm2008	1900	-16.8	17.5	-0.1	4.3
eigen-6c4	1700	-18.5	20.1	0.1	4.4
geco	2100	-14.8	18.5	-0.4	4.9
XGM2016	650	-28.4	37.2	-0.4	8.8
goco05c	700	-28.2	33.9	0.2	8.4
gif48	360	-45.8	58.7	-0.1	15.5
ggm05c	350	-45.4	63.8	0.3	16.6
ITU-GGC16	260	-53.9	75.8	-0.5	21.0
go-cons-gcf-2-tim-r5	260	-52.5	74.3	0.5	21.7
goco05s	260	-53.9	73.1	-0.4	21.8
NULP-02s	220	-92.6	78.1	-0.8	23.0
eigen-6s4-v2	270	-55.8	77.2	-0.7	22.7
egm96	360	-54.9	77.3	-0.2	17.6
Tongji-Grace02s	170	-94.5	69.0	-0.4	22.3
ITSG-Grace2014s	180	-93.1	74.9	-0.5	22.7
HUST-Grace2016s	160	-90.5	75.5	1.0	24.7
ITU-GRACE16	150	-81.1	108.7	-0.7	28.8

Table 8: Statistics of $\delta N = N_{GNSS/lev.} - N_{GGM}$. Units: [cm].

Development of the surface crustal density models

Description

- crucial in achieving *cm* geoid model
- mostly ignored in the past and replaced by some representative constant value
- inversion methods
- developed from gravity, seismic, geological data

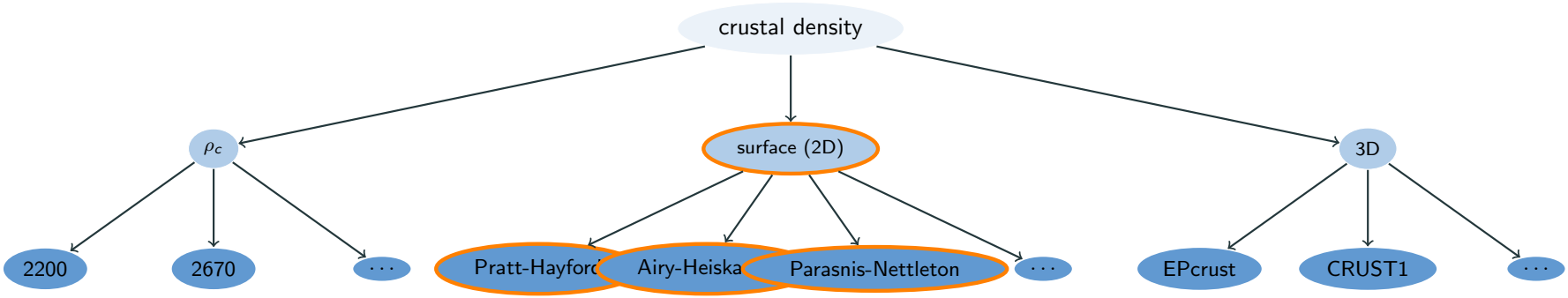

Considerations

- What is the most optimal constant crustal density value, surface model, and 3D model?
- In what way do they improve regional gravity field modeling and geoid model?

Development of the surface crustal density models

Pratt-Hayford's inversion

continent: $\rho_c^{P-H} = \frac{D\rho_0}{D+H}$

sea: $\rho_c^{P-H} = \frac{D\rho_0 - H'\rho_w}{D-H'}$

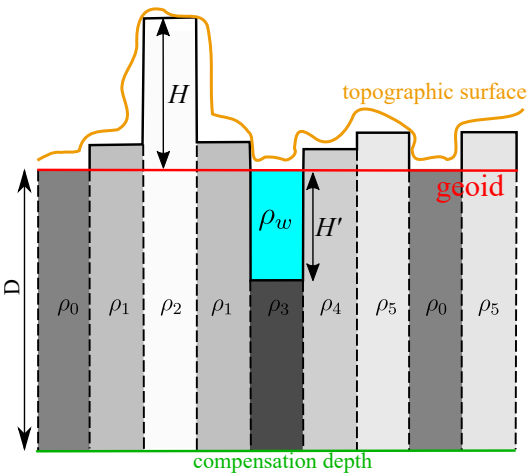

Figure 14: Pratt-Hayford

Airy-Heiskanen's inversion

continent: $\rho_c^{A-H} = -\frac{\rho_m(H-T+T_0)}{T-T_0}$

sea: $\rho_c^{A-H} = -\frac{H'\rho_w - \rho_m(H'+T-T_0)}{T-T_0}$

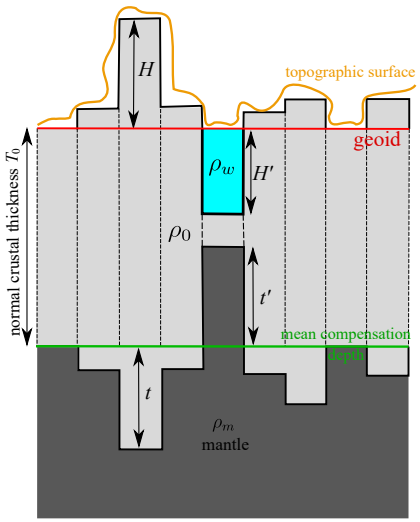

Figure 15: Airy-Heiskanen

Parasnis-Nettletons's inversion

$\Delta g_{sB} = \Delta g_{FA} - 2\pi G\rho H = \Delta g_{FA}$

$a = \frac{\sum_{i=1}^{n}(H_i - \overline{H})(\Delta g_i - \overline{\Delta g})}{\sum_{i=1}^{n}(H_i - \overline{H})^2}$

$\rho_c = \frac{a}{2\pi G H}$

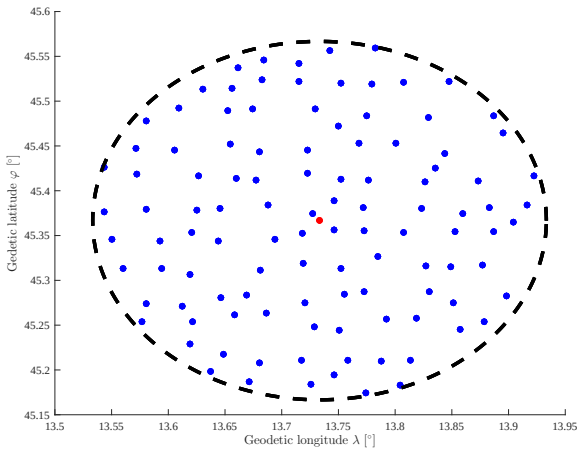

Figure 16: Selection of gravity anomalies

Inversion method	Symbol	Input values
Pratt-Hayford	ρ_0	2300, 2400, 2500, 2670, 2800, 2900, 3000
	D	80, 90, 100, 110, 120, 130, 150
Airy-Heiskanen	ρ_m	2700, 2800, 2900, 3000, 3100, 3200, 3270, 3400, 3500
	T	from CRUST1 model
Parasnis-Nettleton	RS	0.05, 0.1, 0.2, 0.3, 0.5, 0.7, 1.0, 2.0
	n_{max}	0, 5, 10, 30, 50, 100, 200, 500

Table 9: Input parameters

Development of the surface crustal density models

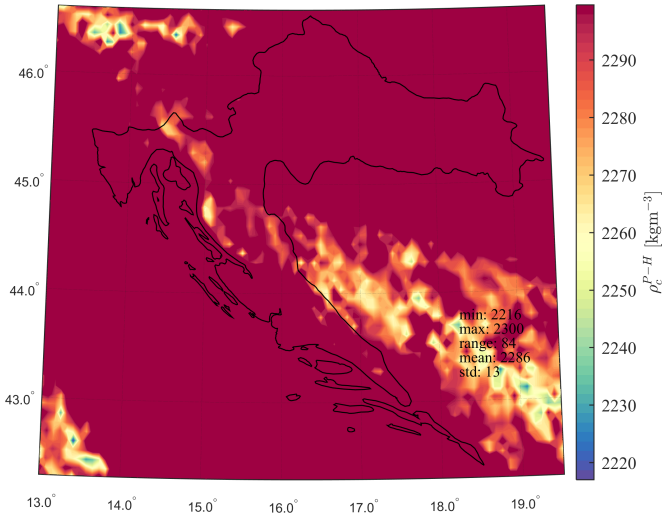

(a) Pratt-Hayford ρ_c^{P-H}

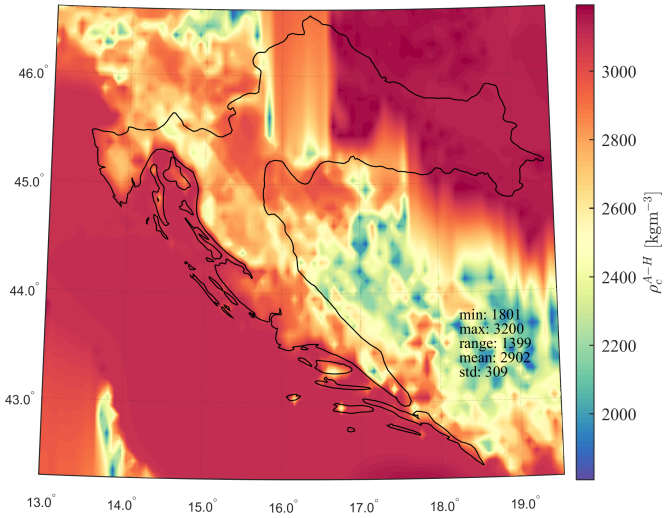

(b) Airy-Heiskanen ρ_c^{A-H}

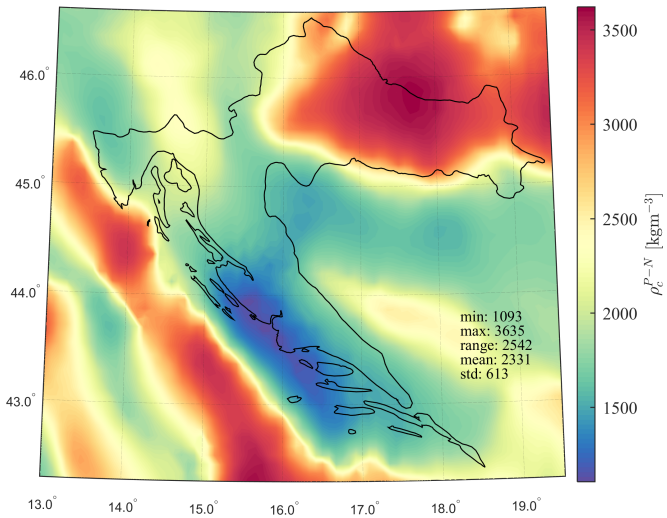

(c) Parasnis- Nettleton ρ_c^{P-N}

Figure 17: Developed models

KTH approach geoid

Considerations

- Compute optimal gravimetric and hybrid geoid models based on input data and models.
- Investigate geoid accuracy when crustal density is changed.
- Investigate geoid accuracy depending of the all possible input data, models and parameters.

Data and parameter name	Acronym	Input values
free air gravity anomalies	Δg_{FA}	gridded gravity database
global geopotential model	GGM	ITU GRACE16, goco05s, goconsgcf2timr5, egm2008,
digital elevation model	DEM	SRTM3, SRTM30, GTOPO30, ETOPO1
constant crustal density (1D)	ρ_c	2000, 2100, ..., 3000 [kgm^{-3}]
density model (2D)	$DDM2$	Airy, Pratt, Parasnis-Nettleton
variance of terrestrial gravity anomalies	C_0	1, 2, 3, ..., 20 [mgal]
kernel type of stochastic Stokes' integral	v	1: optimum, 2: biased, 3: unbiased
spherical cap size	ψ_0	0.1, 0.2, ..., 2.0 [°]
integration radius of gravity gradients in DWC	ψ_{DgR}	0.1, ..., 1.0 [°]
input models (gravity, DEM) resolution	inp mod res	0.01, 0.02, ..., 0.1 [°]
output geoid resolution	geoid res	0.01, ..., 0.2 [°]
gridding method of digital elevation model	DEM grid meth	nearest neighbour, bilinear, bicubic
gridding method of gravity anomalies	anmly grid meth	bilinear, cubic, nearest neighour

Table 10: Input data and parameters for computation of geoid by KTH approach

KTH approach geoid

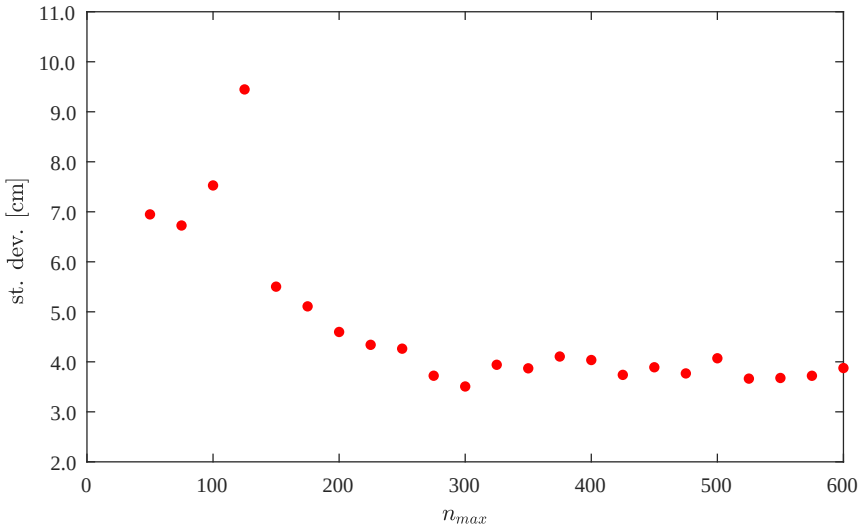

(a) maximum degree of GGM

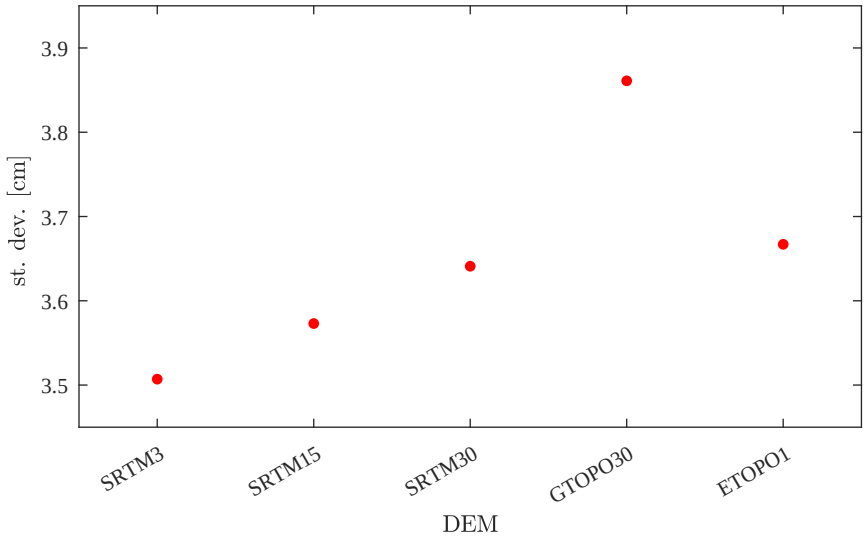

(b) digital elevation model

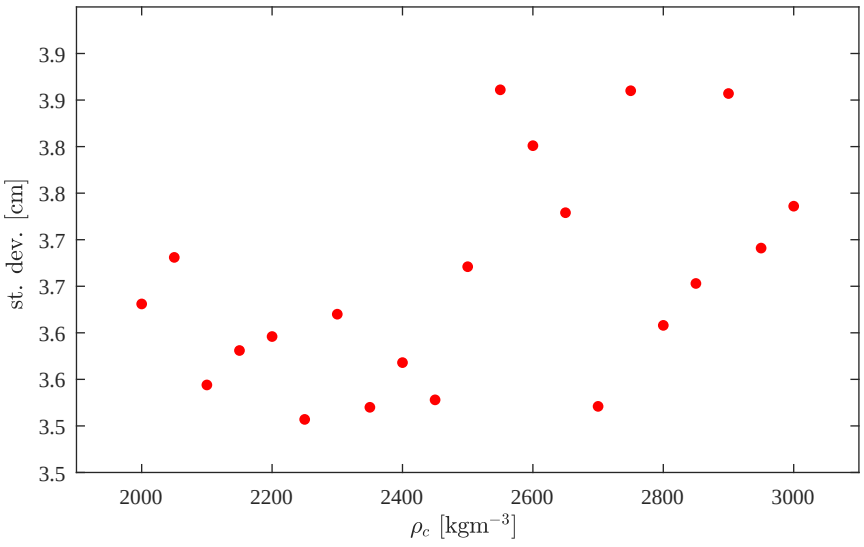

(c) density of the crust

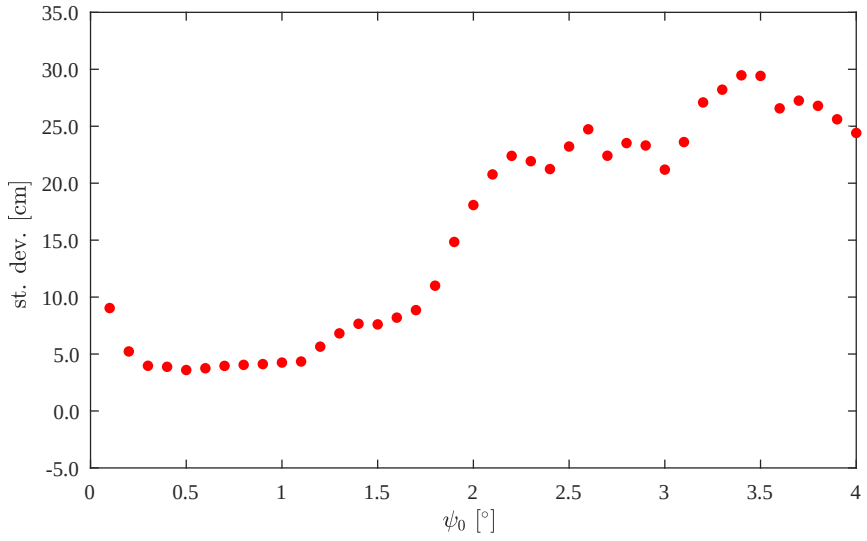

(d) spherical cap size

Figure 18: Geoid accuracy as a function of...

KTH approach geoid

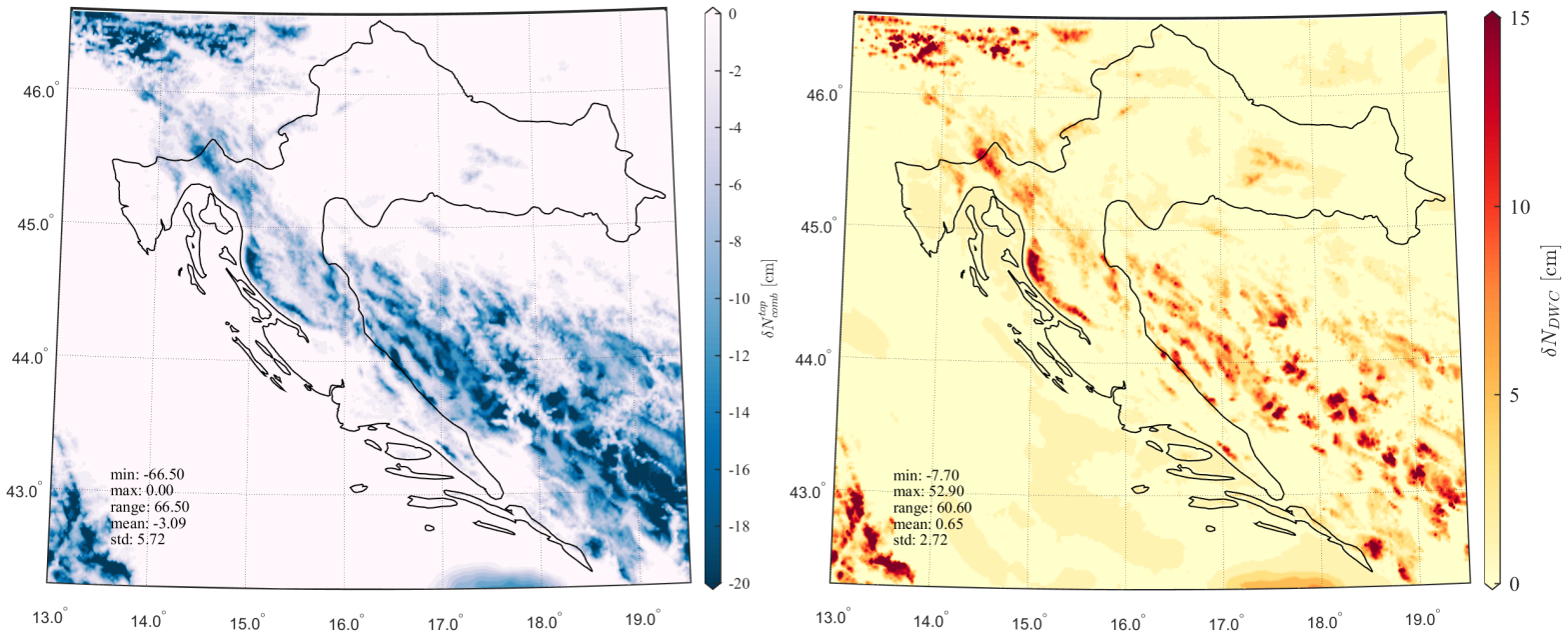

(a) δN^{top}_{comb} (b) δN_{DWC}

Figure 19: Additive corrections

	Units	min	max	range	mean	st. dev.
$\widetilde{N}$	[m]	37.53	50.53	12.99	45.00	2.06
δN_{top}	[cm]	-66.50	0.00	66.50	-3.09	5.72
δN_{DWC}	[cm]	-7.70	52.90	60.60	0.65	2.72
δN_{atm}	[cm]	-0.60	0.30	0.90	-0.06	0.10
δN_{ell}	[cm]	-0.20	0.20	0.40	-0.07	0.05
N	[m]	37.54	50.43	12.89	44.98	2.05

Table 11: KTH approach additive corrections

HRG2018-KTH

selected solution by RMS	fit par	min	max	range	mean	st. dev.
HRG2018-KTH-gra	no fit	-99	-71	28	-87.3	4.8
RG2018-KTH-hyb	3rdpoly	-12	13	25	0.0	3.5

Table 12: Accuracy of HRG2018-KTH geoid models. Selected among more than 3000 different solutions. Units: [cm].

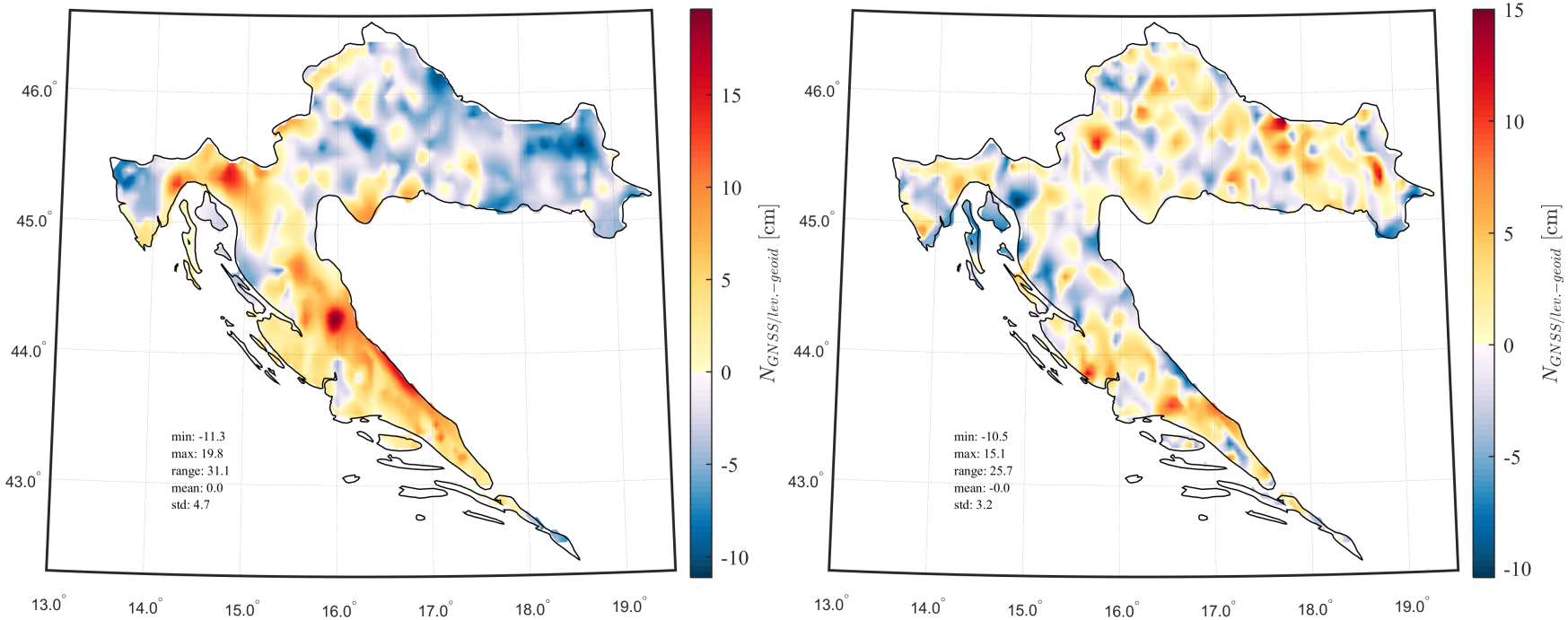

(a) gravimetric after removal of mean -87.3 cm (b) hybrid

Figure 20: Gridded geoid undulation differences $\delta N_{GNSS\,/\,lev.\,-\,geoid}$

Remove-compute-restore approach geoid: methods

Geoid computation method	Acronym
Stokes integration (analytic)	Stokes
LSC (spherical, 3D)	GEOCOL
LSC (planar, 2D)	GPCOL
Planar FFT	GEOFOUR
Spherical multi-band FFT	SPFOUR
Spherical 1D FFT	SP1D

Table 13: RCR methods

RCR approach geoid: input parameters and models

Data and parameter name	Acronym	Input values
residual gravity anomalies	$\Delta g_{FA-GGM-RTM}$	
Stokes' kernel modification	$Stokes_{mod}$	0: no 1: WG, 2: HG, 3: Meissl, 4: VK, 5: sph M-M
degree of Stokes' kernel modification	n_{mod}	10, . . . , 500
inner zone integration range	ψ_{in}	0.25, . . . , 2.0 [°]
outer zone integration range	ψ_{out}	3, 4, 5 [°]

Table 14: Input data and parameters for Stokes method

Data and parameter name	Acronym	Input values
residual gravity anomalies	$\Delta g_{FA-GGM-RTM}$	
tapering windowing width	*iwndow*	0, 1, . . . , 30 [grid points]
remove mean from data	*lmean*	1: yes, 0: no

Table 15: Input data and parameters for GEOFOUR method

no.	min	max	range	mean	st. dev.	inp par
1	-54.2	54.0	108.2	-0.2	14.5	$Stokes_{mod}$= 1, ψ_{in}= 0.3°, ψ_{out}= 3.0°, n_{mod}= 200, GGM= goco05s, n_{max}= 225, dens model= konst, ρ_c= 2670 kgm^{-3} , DEM= SRTM3, DEM grid meth= NEAREST NEIGHBOR, res fine DEM= 5′′, res coarse DEM= 10′′, res ref DEM= 385′′, LPFref DEM= 25′′, r_1= 10 km , r_2= 150 km
2	-16.2	12.9	29.0	0.0	3.8	$Stokes_{mod}$= 2, ψ_{in}= 0.1°, ψ_{out}= 1.0°, n_{mod}= 200, GGM= egm2008, n_{max}= 2190, dens model= konst, ρ_c= 2300 kgm^{-3} , DEM= SRTM30, DEM grid meth= NEAREST NEIGHBOR, res fine DEM= 5′′, res coarse DEM= 25′′, res ref DEM= 30′′, LPFref DEM= 80′′, r_1= 5 km , r_2= 30 km
3	-16.9	13.4	30.3	-0.0	3.7	$Stokes_{mod}$= 4, ψ_{in}= 0.1°, ψ_{out}= 1.0°, n_{mod}= 400, GGM= egm2008, n_{max}= 2190, dens model= konst, ρ_c= 2300 kgm^{-3} , DEM= SRTM30, DEM grid meth= NEAREST NEIGHBOR, res fine DEM= 5′′, res coarse DEM= 10′′, res ref DEM= 30′′, LPFref DEM= 80′′, r_1= 5 km , r_2= 20 km
4	-14.1	12.8	26.9	0.0	3.8	$Stokes_{mod}$= 3, ψ_{in}= 0.1°, ψ_{out}= 1.0°, n_{mod}= 0, GGM= egm2008, n_{max}= 2190, dens model= CRUST1, ρ_c= NaN kgm^{-3} , DEM= SRTM30, DEM grid meth= NEAREST NEIGHBOR, res fine DEM= 5′′, res coarse DEM= 25′′, res ref DEM= 30′′, LPFref DEM= 80′′, r_1= 5 km , r_2= 30 km

Table 16: Accuracy of geoid models developed by Stokes method. 3rdpoly fit. Units: [cm].

no.	min	max	range	mean	st. dev.	inp par
1	-10.9	8.4	19.4	-0.0	3.0	*lmean*= 0, *iwndow*= 40, GGM= egm2008, n_{max}= 2190, dens model= konst, ρ_c= 2300 kgm^{-3} , DEM= SRTM30, DEM grid meth= NEAREST NEIGHBOR, res fine DEM= 5′′, res coarse DEM= 10′′, res ref DEM= 30′′, LPFref DEM= 80′′, r_1= 5 km , r_2= 20 km
2	-9.2	12.5	21.7	0.0	3.1	*lmean*= 0, *iwndow*= 10, GGM= egm2008, n_{max}= 2190, dens model= Pratt, ρ_c= NaN kgm^{-3} , DEM= SRTM30, DEM grid meth= NEAREST NEIGHBOR, res fine DEM= 5′′, res coarse DEM= 25′′, res ref DEM= 30′′, LPFref DEM= 80′′, r_1= 5 km , r_2= 30 km
3	-9.7	12.3	22.0	-0.0	3.1	*lmean*= 0, *iwndow*= 34, GGM= egm2008, n_{max}= 2190, dens model= CRUST1, ρ_c= NaN kgm^{-3} , DEM= SRTM30, DEM grid meth= NEAREST NEIGHBOR, res fine DEM= 5′′, res coarse DEM= 25′′, res ref DEM= 30′′, LPFref DEM= 80′′, r_1= 5 km , r_2= 30 km
4	-10.5	8.8	19.4	0.0	3.0	*lmean*= 0, *iwndow*= 20, GGM= egm2008, n_{max}= 2190, dens model= Pratt, ρ_c= NaN kgm^{-3}, DEM= SRTM30, DEM grid meth= NEAREST NEIGHBOR, res fine DEM= 5′′, res coarse DEM= 10′′, res ref DEM= 30′′, LPFref DEM= 80′′, r_1= 5 km , r_2= 20 km

Table 17: Accuracy of geoid models developed by GEOFOUR method. 3rdpoly fit. Units: [cm].

Comparison of geoid computation approaches and methods

Geoid computation method	min	max	range	mean	st dev
KTH	-11.4	12.1	23.5	-0.2	3.4
Stokes	-16.8	12.8	29.5	-0.0	3.7
GEOFOUR	-9.7	12.3	22.0	-0.0	3.0
GPCOL	-10.6	10.8	21.4	0.1	3.1
SPFOUR	-17.3	13.0	30.4	0.0	3.7
GEOCOL	-10.6	9.1	19.7	0.1	3.1
SP1D	-16.6	11.7	28.3	-0.0	3.6

Table 18: Comparison of geoid models accuracy. Fit: 3rdpoly, units: [cm].

HRG2018-RCR

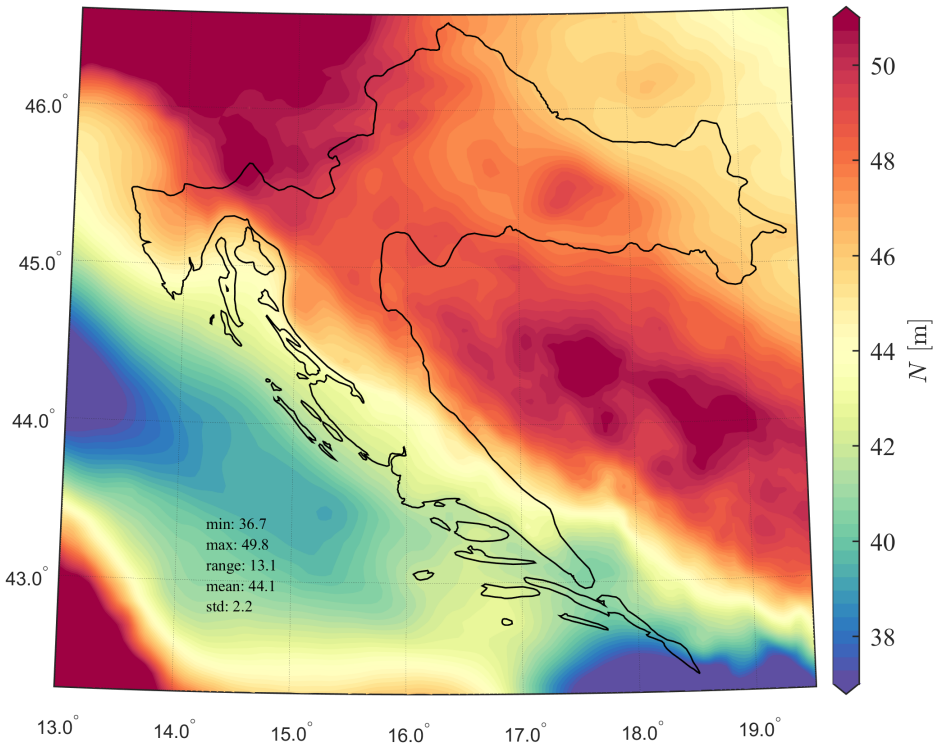

(a) HRG2018-RCR

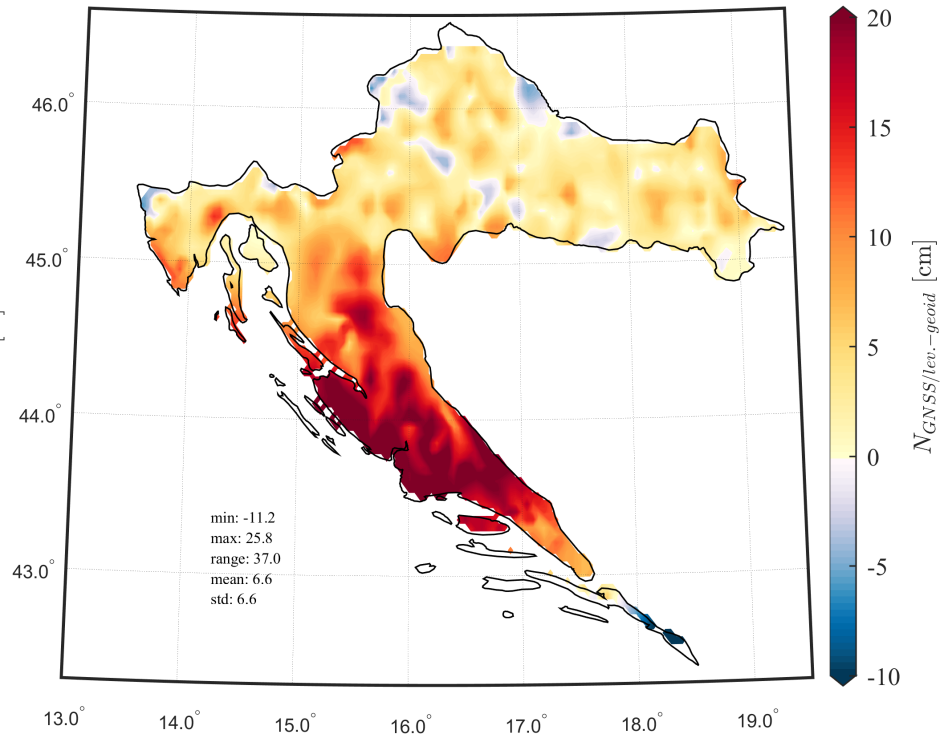

(b) Gridded geoid undulation differences $\delta N_{GNSS\,/\,lev.-geoid}$

HRG2018-RCR: relative geoid accuracy

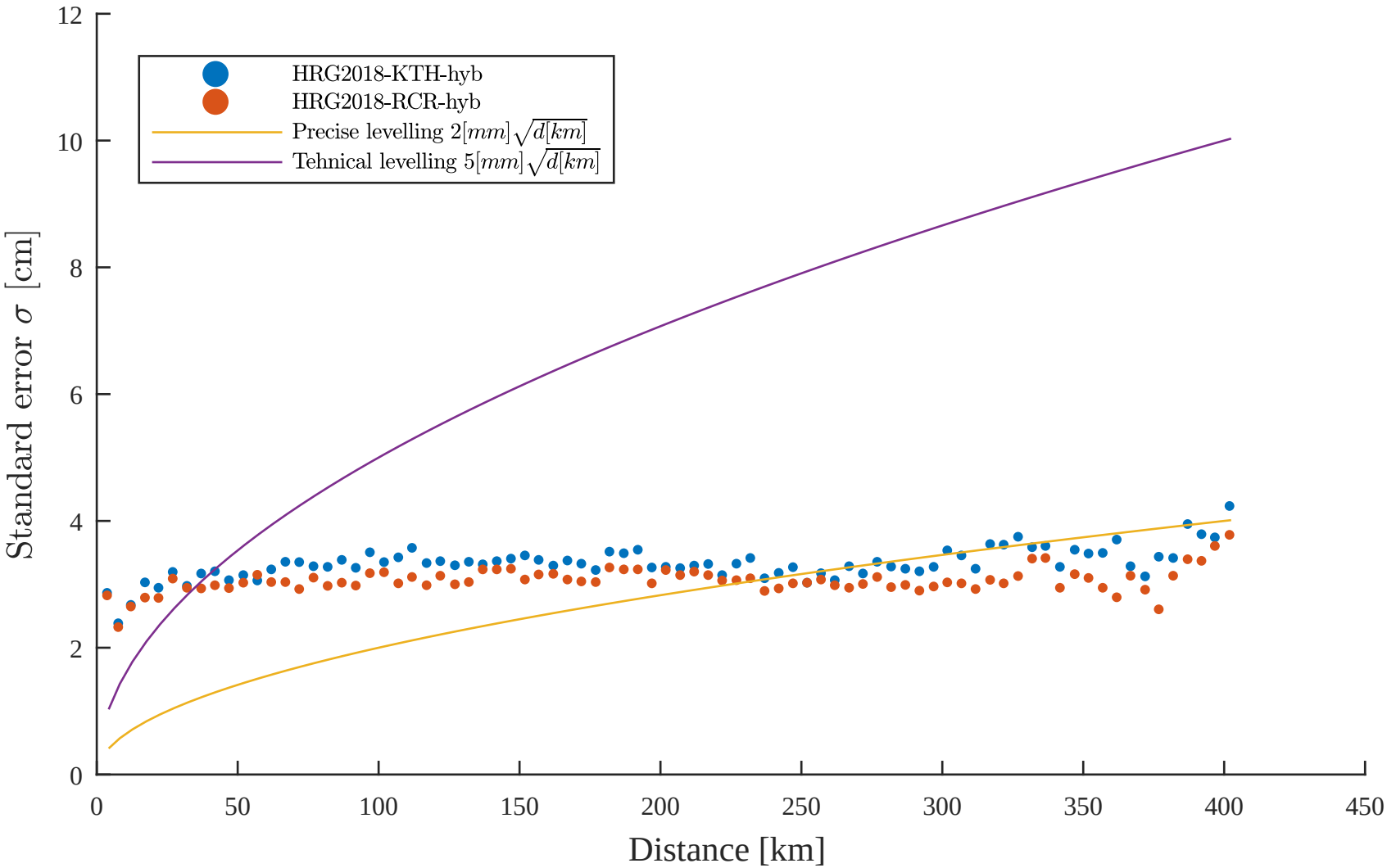

Figure 21: Relative geoid accuracy of hybrid models HRG2018-RCR and HRG2018-KTH

RCR vs KTH approach geoid

Geoid method	min	max	range	mean	st. dev.
KTH - Stokes	36.1	117.0	80.5	91.8	10.2
KTH - GEOFOUR	28.9	133.0	104.0	92.7	12.8
KTH - GPCOL	45.8	141.0	95.4	102.0	15.5
KTH - SPFOUR	31.7	114.0	82.2	88.3	9.7
KTH - GEOCOL	39.9	147.0	107.0	101.0	16.9
KTH - SP1D	32.0	114.0	82.1	88.4	9.6
Stokes - GEOFOUR	-14.8	25.3	40.1	0.9	7.5
Stokes - GPCOL	-8.0	34.2	42.2	9.6	9.2
Stokes - SPFOUR	-16.0	5.9	21.8	-3.5	4.1
Stokes - GEOCOL	-14.8	40.2	54.9	9.0	11.3
Stokes - SP1D	-15.6	4.0	19.6	-3.4	3.6
GEOFOUR - GPCOL	-7.0	34.5	41.5	8.8	8.8
GEOFOUR - SPFOUR	-39.4	16.5	55.9	-4.4	10.5
GEOFOUR - GEOCOL	-12.8	38.1	50.9	8.2	8.0
GEOFOUR - SP1D	-35.1	15.4	50.5	-4.3	9.8
GPCOL - SPFOUR	-47.3	9.3	56.6	-13.1	12.7
GPCOL - GEOCOL	-29.1	17.1	46.2	-0.6	6.3
GPCOL - SP1D	-46.1	7.0	53.1	-13.0	12.4
SPFOUR - GEOCOL	-13.9	54.1	67.9	12.5	15.0
SPFOUR - SP1D	-3.0	4.8	7.8	0.1	1.3
GEOCOL - SP1D	-52.4	13.5	65.9	-12.4	14.6

Table 19: Statistics of the differences ($\delta N = grid - grid$) between gravimetric geoid models computed using different computation methods. Units: [cm].

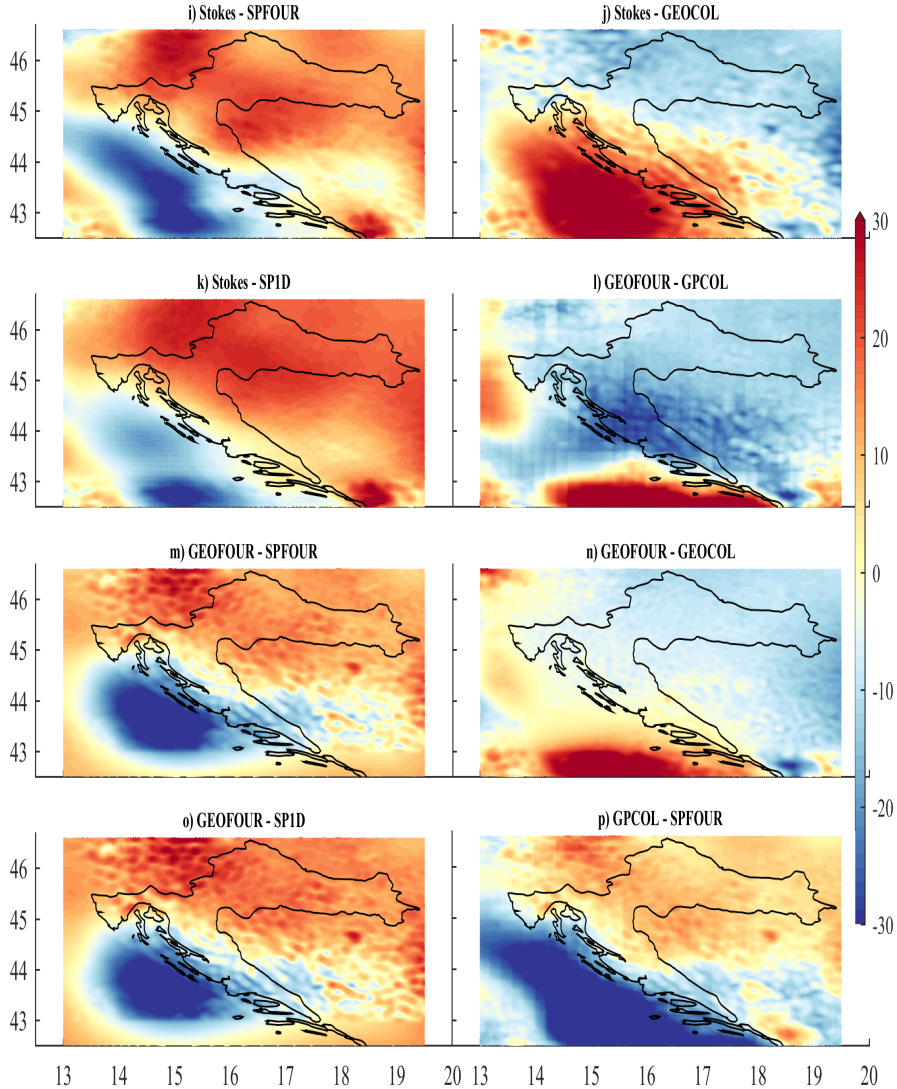

Figure 22: Differences (*grid 1 — grid 2*) between gravimetric geoid models calculated by using different computation methods. Units: [cm]. Part 1/3.

Influence of crustal density on geoid accuracy

crustal parameter/model		min	max	range	mean	st. dev.
1D	$\rho_c = 2000$	-14	15	29	1.6	5.7
	$\rho_c = 2100$	-14	14	29	1.0	5.1
	$\rho_c = 2200$	-15	14	28	-0.4	5.3
	$\rho_c = 2300$	-16	13	29	-1.5	5.4
	$\rho_c = 2400$	-16	13	29	-2.2	5.5
	$\rho_c = 2500$	-16	13	29	-3.2	6.1
	$\rho_c = 2600$	-17	13	29	-3.9	6.2
	$\rho_c = 2670$	-18	13	31	-4.7	6.1
	$\rho_c = 2700$	-19	13	31	-5.1	6.4
	$\rho_c = 2800$	-21	13	34	-6.0	6.9
	$\rho_c = 2900$	-24	13	36	-6.9	7.2
	$\rho_c = 3000$	-26	13	39	-8.1	7.8
	$\rho_c = 3100$	-29	13	41	-9.3	8.0
2D	CRUST1	-16	14	31	-2.0	5.6
	EPcrust	-15	15	30	0.3	5.2
	Airy-Heiskanen	-18	14	32	-4.3	6.8
	Parasnis-Nettleton	-15	15	30	1.2	5.7
	Pratt-Hayford	-14	14	29	1.1	5.2
3D	CRUST1	-16	14	31	-1.5	5.0
	EPcrust	-15	14	29	0.3	4.9

Table 20: The accuracy of gravimetric geoid models computed with constant values, 2D surface (lateral) and 3D crustal models. Units: ρ_c in [kgm^{-3}], statistics in [cm].

crustal parameter/model		min	max	range	mean	st. dev.
1D	$\rho_c = 2000$	-9	7	17	0.1	3.3
	$\rho_c = 2100$	-9	8	18	0.1	3.1
	$\rho_c = 2200$	-10	9	19	-0.2	3.3
	$\rho_c = 2300$	-10	9	18	-0.2	3.5
	$\rho_c = 2400$	-10	9	18	-0.2	3.5
	$\rho_c = 2500$	-9	9	18	-0.2	3.5
	$\rho_c = 2600$	-10	9	18	0.0	3.4
	$\rho_c = 2670$	-9	10	19	0.0	3.4
	$\rho_c = 2700$	-9	9	18	0.1	3.2
	$\rho_c = 2800$	-10	9	20	0.0	3.5
	$\rho_c = 2900$	-18	10	28	0.1	3.9
	$\rho_c = 3000$	-9	10	20	0.1	3.6
	$\rho_c = 3100$	-11	9	20	0.0	3.5
2D	CRUST1	-8	10	18	0.3	3.2
	EPcrust	-9	7	17	-0.4	3.5
	Airy-Heiskanen	-12	8	19	-0.1	3.4
	Parasnis-Nettleton	-9	8	17	0.1	3.3
	Pratt-Hayford	-8	8	16	0.3	3.1
3D	CRUST1	-8	9	18	0.3	3.0
	EPcrust	-9	7	16	-0.3	3.0

Table 21: The accuracy of hybrid (fitted) geoid models computed with constant values, 2D surface (lateral) and 3D crustal models. Units: ρ_c in [kgm^{-3}], statistics in [cm].

Comparison of fitting parametric models

fit model	min	max	range	mean	st. dev.
nofit	-13.0	36.8	49.9	8.6	9.9
bias	-22.1	28.5	50.6	0.1	9.9
linear	-35.2	16.9	52.1	-0.2	6.8
2ndpoly	-10.6	11.9	22.6	-0.1	3.6
3rdpoly	-9.7	12.3	22.0	-0.0	3.0
3pfit	-34.9	16.7	51.7	-0.2	6.7
4pfit	-24.9	17.3	42.1	-0.2	5.8
5pfit	-21.2	16.6	37.8	-0.2	5.6
7pfit	-9.7	14.3	24.0	-0.1	3.3

Table 22: Statistics of GEOFOUR geoid solution by different fitting parametric models. Units: [cm].

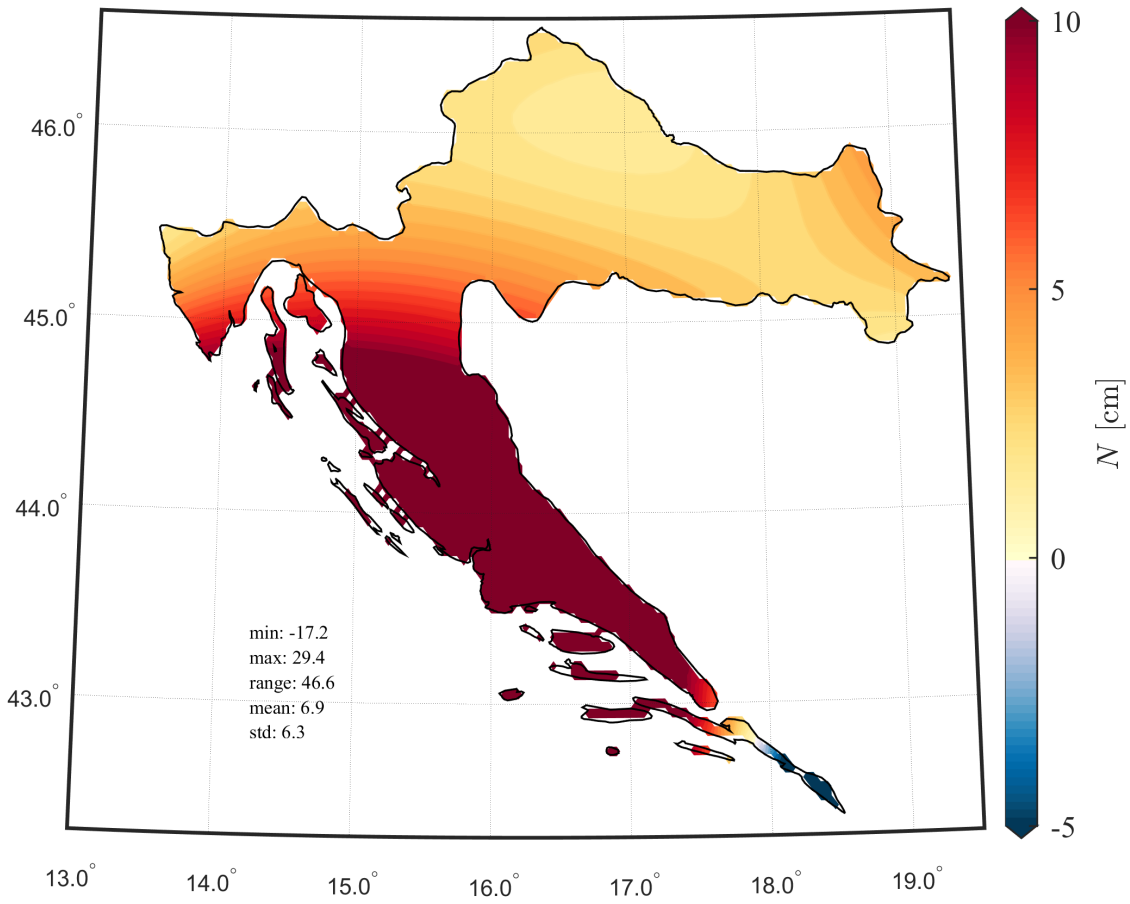

Figure 23: Transformation surface: difference between gravimetric and hybrid HRG2018-RCR models

Models of gravity anomalies and topographic reductions

Model of	min	max	range	mean	st. dev.
Δg_{FA}	-59	120	178	13	23
δg_{TC}	-0	21	21	2	3
Δg_{Faye}	-48	125	173	15	22
Δg_{sB}	-90	45	135	-18	26
Δg_{cB}	-84	47	131	-16	25
δg_{A-H}	-1	256	257	59	52
Δg_{A-H}	-187	39	226	-46	46

Table 23: Statistics of the gravity anomaly models. Units: [mgal].

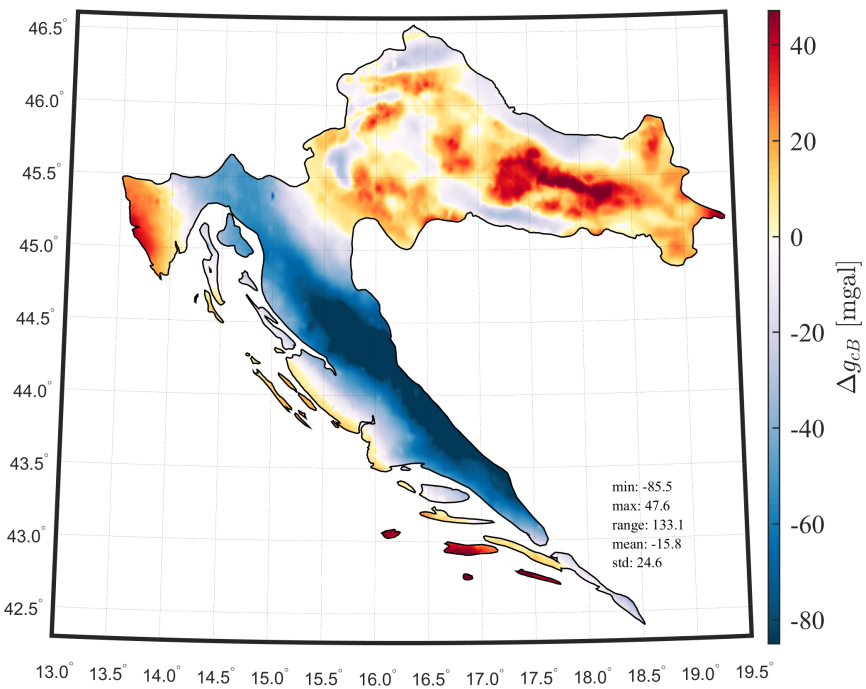

(a) Complete Bouguer anomaly Δg_{cB} model

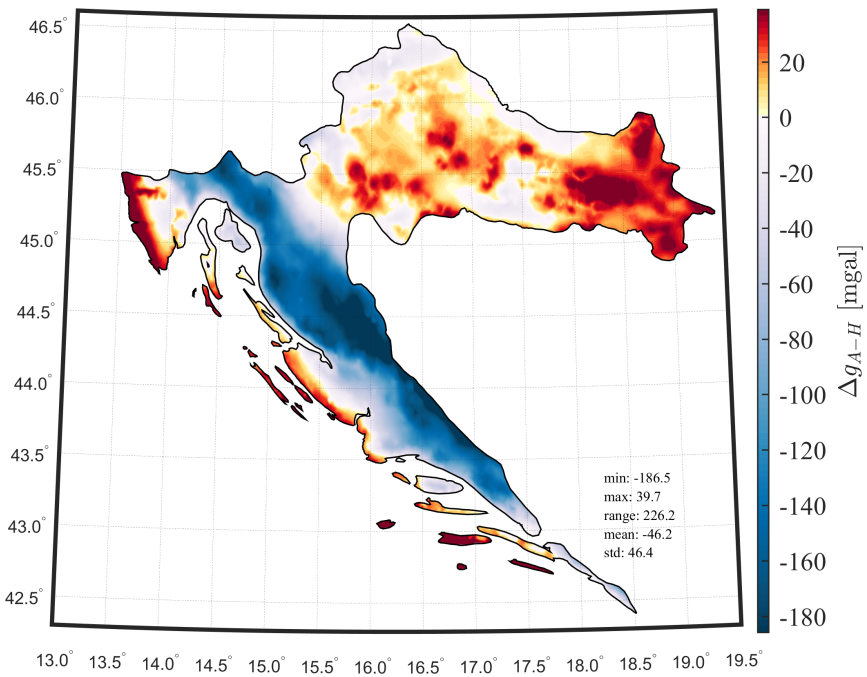

(b) Airy-Heiskanen t-i anomaly Δg_{A-H} model

Developed software

Summary

- Programming languages: Fortran, Matlab, C++
- No. of scripts: 160.
- No. of code lines: 13.260

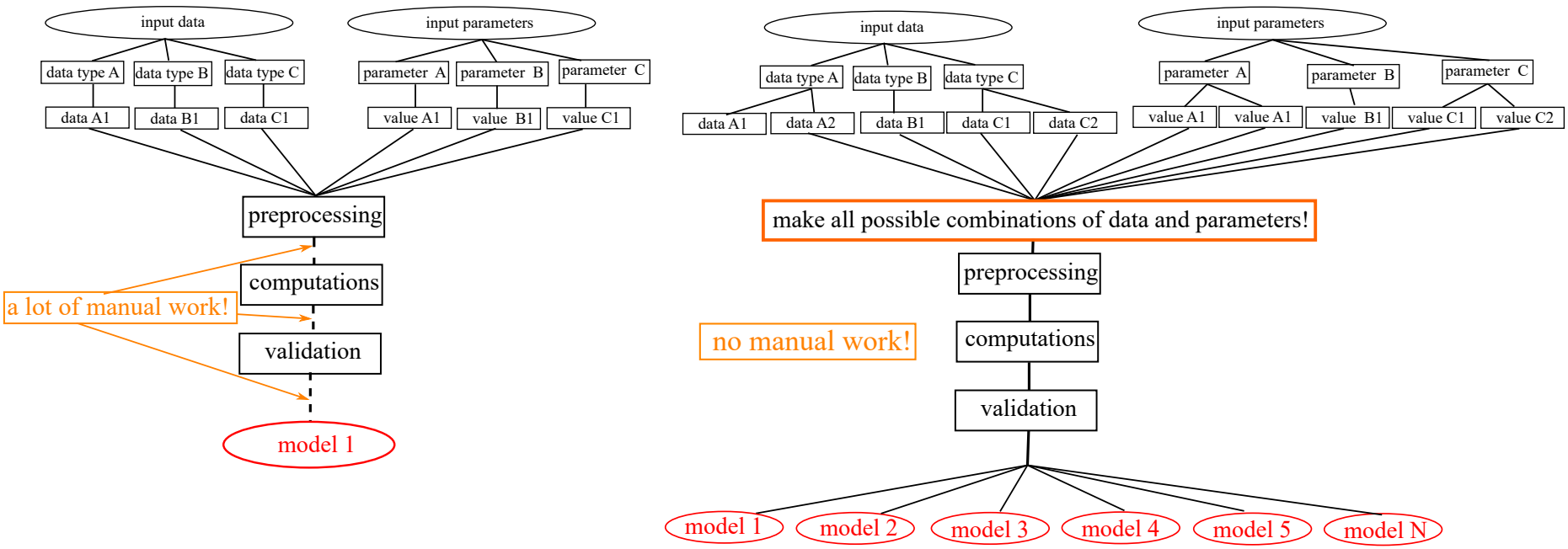

Figure 24: Flowchart of gravity field modelling and geoid computation process. Before (left), after (right)

Scientific contribution and conclusions of the thesis

1. Methodology for inclusion of 2D and 3D crustal density models.
2. Automatized methodology allowing seamless gravity field modeling and geoid determination.
3. Surface crustal density models for the Republic of Croatia.
4. Assessment of the influence of crustal density models, and all input parameters and models on the accuracy of geoid models.
5. Optimal selection and estimates of the:
   - constant crustal density value,
   - satellite and combination-data GGM model,
   - gravity anomalies gridding method.
6. Improved gravimetric and hybrid geoid models for the Republic of Croatia.
7. Implementation, analysis and comparison of the main geoid determination approaches and methods.

Further research

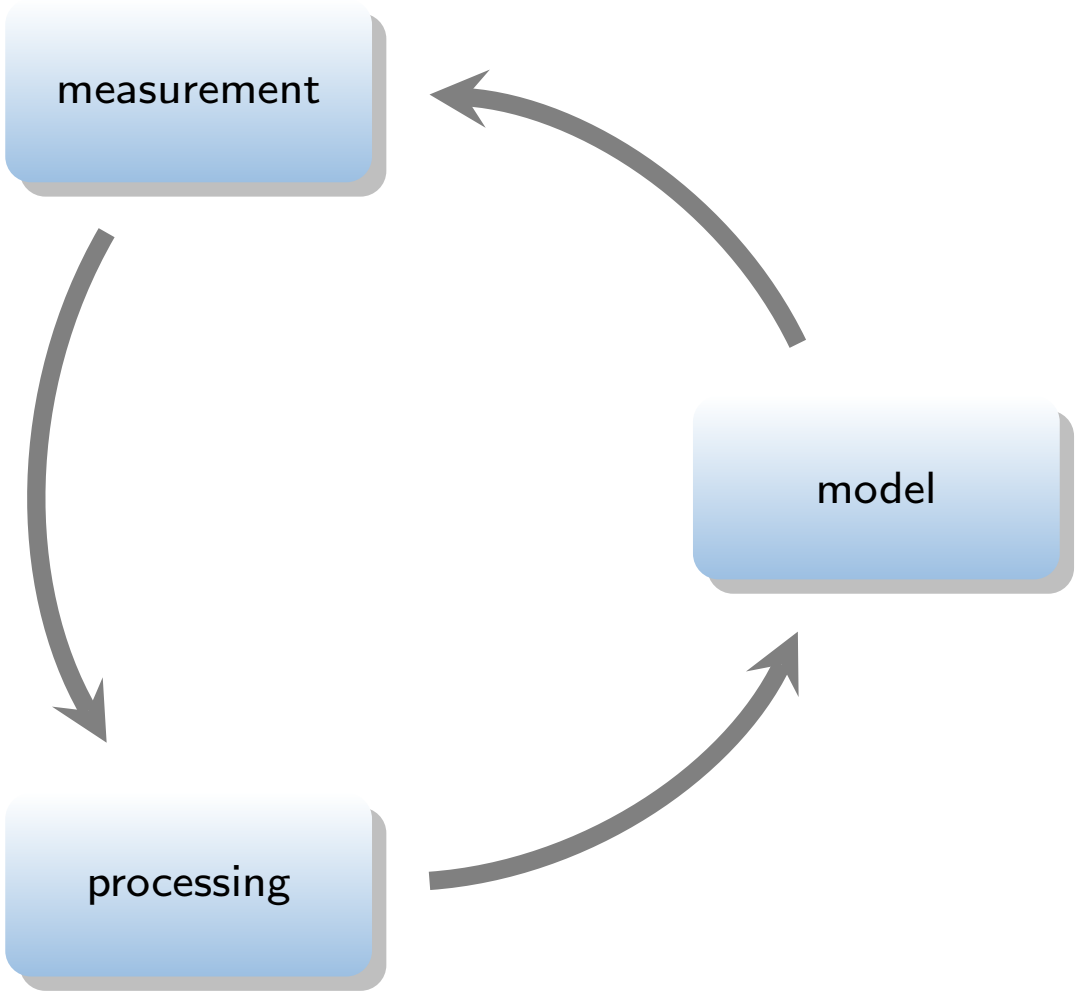

"All models are wrong, but some are useful." (G.B.)

Thank you kindly for your attention!

References

Bašić, T., & Bjelotomić, O. (2014). Hrg2009: New high resolution geoid model for croatia. In *Gravity, Geoid and Height Systems* (pp. 187–191). Springer.

Bjelotomić, O. (2015). *High resolution geoid modelling of croatia* (PhD thesis). Faculty of Geodesy, University of Zagreb.

Brkić, M. (1994). *An improved method of earth's crust masses modelling for geodetic and geophysical purposes* (MSc thesis). Faculty of Science, Department of Geophysics, University of Zagreb.

Fotopoulos, G. (2013). Combination of heights. *Geoid Determination*, 517–544.

Gerlach, C. (2003). *Zur höhensystemumstellung und geoidberechnung in bayern* (Unpublished doctoral dissertation). Bayerischen Akademie der Wissenschaften.

Nagy, D. (1966). The prism method for terrain corrections using digital computers. *Pure and Applied Geophysics*, *63*(1), 31–39.